Valdemar Rebelo Duarte

Licenciado em Ciências de Engenharia Mecânica

Additive manufacturing of a high resistance steel by MIG/MAG

Dissertação para obtenção do Grau de Mestre em Engenharia Mecânica

Orientadora: Professora Doutora Rosa Maria Mendes Miranda, Professora Associada com Agregação, Universidade Nova de Lisboa

Co-Orientador: Doutor João Pedro de Sousa Oliveira, Universidade Nova de Lisboa

FACULDADE DE CIÊNCIAS E TECNOLOGIA
UNIVERSIDADE NOVA DE LISBOA

Julho 2016

Additive manufacturing of a high resistance steel by MIG/MAG

To my family

Acknowledgments

First, I would like to express my sincere gratitude to my supervisor Professor Rosa Miranda for her unwavering support and guidance throughout this work, the opportunities given and the vote of confidence.

I am also most grateful to Doctor João Oliveira for the XRD analysis and for being always available to help and to advise.

I gratefully acknowledge Eng. Hugo Costa from Lincoln Electric, for providing the consumable material.

My sincere thanks to Prof. Rui Silva from CENIMAT for SEM observations in such a short time and to Prof. Alexandre Velhinho for the guidance on the microscope manipulation.

I also wanted to thank Prof. Telmo Santos for advice and assistance in the development of the data acquisition system and Prof. Carla Machado.

My sincerely thank Mr. António Campos and Mr. Paulo Magalhães for always being available to help me during the experimental work.

To my colleagues and dearest friends who always showed their support and companionship, in particular, to André Reis for his help and support in so many different ways.

Finally, my deepest gratitude to my parents, who made possible this accomplishment and for the education given that made me who I am.

Resumo

A produção aditiva é considerada como fazendo parte da 4ª Revolução Industrial na era digital, permitindo avanços no design de produtos, materiais, engenharia de processo e softwares de simulação e transferência de dados. Os desenvolvimentos recentes têm incidido na produção de componentes metálicos com formas complexas, de grandes dimensões com custos reduzidos. Especial destaque tem sido dado às tecnologias de soldadura que usam arco eléctrico como fonte de calor e consumíveis em forma de fio. A elevada taxa de deposição, baixos custos e fácil acessibilidade são as principais razões que despertaram o interesse em *wire and arc additive manufacturing* (WAAM).

Este estudo incidiu sobre a utilização de WAAM para produzir formas simples em aço de baixa liga e alta resistência e caracterização: do processo, das características geométricas e das propriedades mecânicas e estruturais do material depositado. A influência dos parâmetros de processo nas características de deposição foi também estudada.

Concluiu-se que é viável a utilização da tecnologia de soldadura por arco eléctrico para a produção de componentes por WAAM com o material estudado, produzindo-se peças simples sem defeitos internos. Tanto a caracterização mecânica como a estrutural confirmaram a integridade das peças produzidas. Obteve-se uma deposição de material constante, com uma largura de deposição de cerca de 5 mm e uma ondulação de cerca de 110 μm, que são consideravelmente mais baixos do que os resultados apresentados noutros trabalhos com materiais metálicos diferentes do visado neste estudo. Os valores de resistência à tração foram superiores ao especificado pelo fabricante para o material depositado, e são consistentes com a dureza medida, variando entre 800 MPa e 1 GPa, dependendo da entrega térmica. As taxas de deposição obtidas variaram entre 122,9 e 427,5 cm^3/h.

Palavras-chave: produção aditiva, soldadura, soldadura por arco eléctrico, aço de baixa liga e elevada resistência.

Abstract

Additive manufacturing (AM) is considered to be part of the 4th Industrial Revolution in digital era with advances in product design, materials, process engineering and simulation and data transfer software. Recent developments focus in the production of metallic components with more complex shapes, big sizes at reduced costs. Special highlight has been given to welding technologies where the electric arc is the heat source and the consumable wire, the material to deposit. High deposition rate, relatively low costs and accessibility are the main reasons for the interest in wire and arc additive manufacturing (WAAM).

This study focused on using WAAM to produce simple shapes in high strength low alloy steel and characterize: the process, the geometrical features and the mechanical and structural properties of deposited material. The influence of the process parameters on the deposition characteristics was also studied.

It was concluded that arc welding is a feasible technology to produce components by WAAM in the material under study without internal defects. Both mechanical and structural characterization confirmed the integrity of produced parts. A constant material deposition was achieved, with a deposition width of about 5 mm and a waviness around 110 μm, which is very much below reported results for other metallic materials. Tensile strength was above the one specified for the wire and is consistent with hardness measured, ranging from 800 MPa to 1 GPa depending on the heat input. Deposition rates from 122.9 to 427.5 cm^3/h were obtained.

Keywords: additive manufacturing, welding, WAAM, arc welding, high strength steel.

Contents

List of figures

List of tables

Acronyms

3D	Three-dimensional
AM	Additive Manufacturing
CAD	Computer Aided Design
CMT	Cold Metal Transfer
CTWD	Contact Tip to Work Distance
DoE	Design of Experiments
EBM	Electros Beam Melting
EDS	Energy dispersive X-ray Spectrometry
FZ	Fuzion Zone
GFR	Gas Flow Rate
GT	Gas Type
HAZ	Heat Affected Zone
HI	Heat Input
HV	Hardness Vickers
I	Current Intensity
LDM	Laser Metal Deposition
LENS	Laser Engineered Net Shape
MAG	Metal Active Gas
MIG	Metal Inert Gas
RP	Rapid Prototyping
RZ	Re-melted Zone
SEM	Scanning Electron Microscopy
SLM	Selective Laser Melting
SLS	Selective Laser Sintering
TIG	Tungsten Inert Gas
TS	Travel Speed
U	Voltage
UTS	Ultimate Tensile Strength
VA	Voltage Adjustment
WAAM	Wire and Arc Additive Manufacturing
WLAM	Wire and Laser Additive Manufacturing
WFS	Wire Feed Speed
WSG	Weld Shielding Gas

1

Introduction

1.1 Motivation

Nowadays, the industry is facing the challenge of a major demand in terms of delivering times, personalized parts production and high complexity geometry components. Most of the conventional manufacturing processes are not able to answer these requirements due to several limitations, such as: time to produce, waste material, costs, or even lack of capability. Additive manufacturing (AM), especially with metallic materials, has shown to be able to accomplish these demands and is being increasingly studied and applied in industry.

AM is already considered as being part of the 4th industrial revolution due to the possibility of producing free form component with, virtually, any shape.

Amongst the technologies available for additive manufacturing, those using welding have the advantages of requiring non expensive equipment, easy to manipulate, at high deposition rates.

Despite the fact that Laser is the most used technology, electric arc with wire deposition is finding increasing applications but limited studies are available.

1.2 Objectives

This thesis aims to perform a feasibility study of using automated arc welding processes, specifically metal inert gas / metal active gas (MIG / MAG), with wire in the so called wire and arc additive manufacturing (WAAM) to deposit a high strength low alloy steel. This is a steel with about 790 MPa tensile strength, that can be used in parts requiring mechanical resistance associated to a good ductility as the deposited material with this wire has about 20 % elongation.

So, the specific objectives were to:

- produce parts with simple geometries with different process parameters;
- characterize the parts for both structural and mechanical properties;

- analyse geometrical features of parts produced, such as: width, height per layer and waviness.
- assess the effect of processing parameters on the deposition rate to evaluate the productivity.

1.3 Document structure

This thesis is organized in five chapters.

The first one details the motivation and objectives of this study.

Chapter 2 briefly describes the state of the art focusing the wire and arc additive manufacturing of metallic materials.

Chapter 3 describes the experimental procedure adopted.

Chapter 4 discusses and present the results of the experimental work and finally the conclusions and future work is given in chapter 5.

2

Literature review

In this chapter the principal concepts of additive manufacturing (AM) are presented and existing knowledge discussed.

ASTM International has defined additive manufacturing as “a process of joining materials to make objects from 3D model data, usually layer upon layer, as opposed to subtractive manufacturing methodologies”. Several other designations exist to describe this technology such as additive fabrication, additive processes, additive techniques, additive layer manufacturing, layer manufacturing and freeform fabrication [1].

2.1 Additive manufacturing

Additive manufacturing (AM) is used in a broad set of final parts in which are included prototypes (for design verification, form and fit checking), tools, patterns, and concept parts, as well as, functional parts with required properties for direct industrial applications [2]. This process was developed based on the rapid prototype (RP) concept, in order to rapidly build parts and components designed by engineers and test their performance.

The major advantages related to product development are: reduction of time, costs, wasted material, human interaction and, thus the overall product development cycle [3]. Opposite to AM, most of the conventional processes require intermediate steps, such as, manufacturing of specific devices, namely tools and dies or moulds, set up preparation and/or tool changing. A given part can be obtained directly from the 3D CAD model, minimizing errors in production, including human interaction.

For metallic parts, AM has a very competitive position when compared to conventional processes in the production of components with a high geometrical complexity. In industries, as automotive and aerospace, it enables to improve performance and reduce weight, leading to lower fuel consumption and cost reduction. This capability also allows the reduction of the number of components needed to complete an assembly, i.e., the same component with the same functionality can be produced with

less parts, due to the possibility of producing parts with higher geometrical complexity, eliminating the need of joining and forming processes. It also allows to reduce cost related to the achievement of narrow tolerances in single parts, as this does no longer apply.

However, AM has still several restrictions limiting its application. For example, surface finishing, the build space of AM machine, which sets a physical limit to components dimensions and, in some technologies, the quality of the produced parts. Table 2.1 summarizes the main opportunities and limitations of AM from both technological and economical perspectives [4].

Table 2.1 Opportunities and limitations from technological and economical perspectives [4]

Technological characteristics of AM	
Opportunities	**Limitations**
+ Direct digital manufacturing of 3D product designs without the need for tools or Moulds	- Solution space limited to 'printable' materials (e.g., no combined materials) and by size of build space
+ Change of product designs without cost penalty in manufacturing	- Quality issues of produced parts: limited reproducibility of parts, missing resistance to environmental influences
+ Increase of design complexity (e.g., lightweight designs or integrated cooling chambers) without cost penalty in manufacturing	- Significant efforts are still needed for surface finishing
+ High manufacturing flexibility: objects can be produced in any random order without cost penalty	- Lacking design tools and guidelines to fully exploit possibilities of AM
+ Production of functionally integrated designs in one-step	- Low production throughput speed
+ Less scrap and fewer raw materials required	- Skilled labour and strong experience needed
Economic characteristics of AM	
+ Acceleration and simplification of product innovation: iterations are not costly and end products are rapidly available	- High marginal cost of production (raw material costs and energy intensity)
+ Price premiums can be achieved through customization or functional improvement (e.g., lightweight) of products	- No economies of scale
+ Customer co-design of products without incurring cost penalty in manufacturing	- Missing quality standards
+ Resolving "scale-scope dilemma": no cost penalties in manufacturing for higher product variety	- Product offering limited to technological feasibility (solution space, reproducibility, quality, speed)
+ Inventories can become obsolete when supported by make-to-order processes	- Intellectual property rights and warranty related limitations
+ Reduction of assembly work with one-step production of functional products	- Training efforts required
+ Lowering barriers to market entry	- Skilled labour and strong experience needed
+ Local production enabled	

+ Cost advantages of low-wage countries might diminish in the long run

The evolution of materials and processes in AM is strongly connected. The need for additively produce complex materials implies the development of new processes which in turn allows the production of new materials. Concerning the final product, initially AM was mainly used to produce prototypes aiming at the validation of aesthetic aspects, followed by the production of parts to test their functionalities. Nowadays, the focus of AM research is the fabrication of complex-shaped metal parts, in difficult to process materials, such as titanium and nickel-based alloys, that cannot be economically produced using conventional methods [5].

Several challenges arise when communication is required, in both technical and non-technical settings. In order to standardize terminology, ASTM had created different categories where can be fitted the current AM machine technologies and future ones [1]. Table 2.2 shows the 6 categories proposed by ASTM.

Table 2.2 AM categories and their definition according to ASTM [1]

Category	**Definition**
Binder jetting	- an additive manufacturing process in which a liquid bonding agent is selectively deposited to join powder materials.
Directed energy deposition	- an additive manufacturing process in which focused thermal energy is used to fuse materials by melting as they are being deposited.
Material extrusion	- an additive manufacturing process in which material is selectively dispensed through a nozzle or orifice.
Material jetting	- an additive manufacturing process in which droplets of build material are selectively deposited.
Powder bed fusion	- an additive manufacturing process in which thermal energy selectively fuses regions of a powder bed.
Sheet lamination	- an additive manufacturing process in which sheets of material are bonded to form an object.
Photopolymerization	- an additive manufacturing process in which liquid photopolymer in a vat is selectively cured by light-activated polymerization.

2.2 Additive manufacturing with metals

In order to accomplish the demands from several industries namely, aerospace [6,7] , automotive, medical [8,9], rapid tooling and other, an enormous variety of metallic materials and techniques have been developed and used. Some researchers have classified the additive manufacturing processes according to the type of bulk material. Figure 2.1 presents the most widely used AM technologies to produce metallic components.

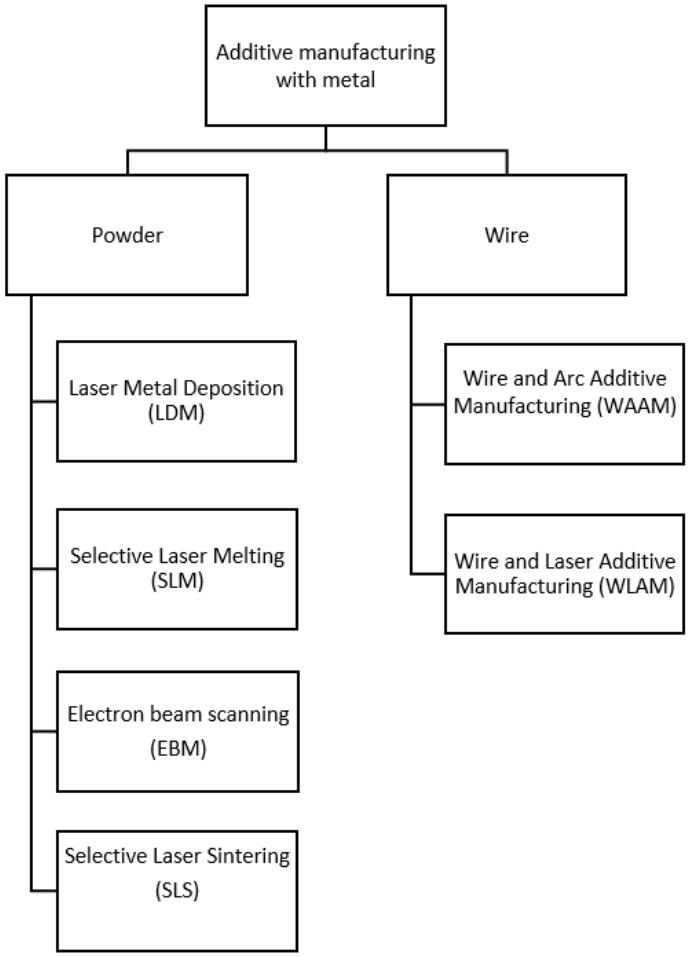

Figure 2.1 Metal additive manufacturing technologies

In the powder-based processes, Selective Laser Sintering (SLS) is an AM process that uses a laser beam to selectively sinter powder particles by scanning cross-sections on the surface of a powder bed layer-by-layer. After each layer the powder bed is scanned, lowered by one-layer thickness and a new layer of powder is spread on top repeating the process until the part is completely built. The powder materials used to produce parts by SLS include polymer/metal powders, metals and ceramics

[2]. In the production of some metal and ceramic parts the powders are mixed with polymer particles acting as a binder, causing a need of post processing to eliminate the binder and fully sinter the part [10]. Gideon et al. [11] reported the use of some advanced materials including IN 718, ZrSiO4, SiC, nickel based alloys, super alloys, copper alloys and hardened tool steel.

Similar to SLS, Selective Laser Melting (SLM) uses a high-power laser to completely melt the metal powder. This can become completely dense and does not require post processing. The mechanical properties of a SLM build part is equal or even better than those of rolled metal sheets. Due to the large energy input to melt metallic particles the process is more difficult to control. Problems such as balling, residual stress and part deformation can occur if the parameters are not well controlled. Stainless steel, cobalt chromium, Inconel and titanium are some of the materials available for this process [2].

Electron Beam Melting (EBM) is also a powder-based process very similar to SLM. The main differences are: the energy source, which is an electron beam rather than a laser beam, and the vacuum chamber where the process takes place. Both EBM and SLS can process a high variety of pre-alloyed metals [3]. SLS, SLM and EBM use a powder bed as the feeding system (Figure 2.2).

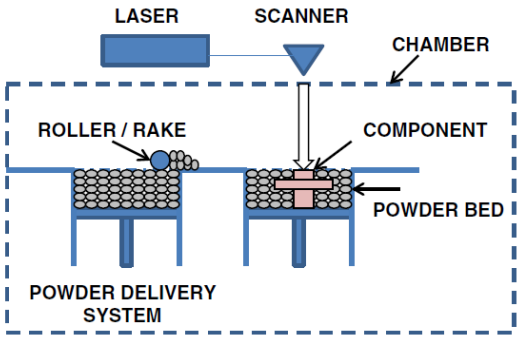

Figure 2.2 Schematic of a powder bed system [12]

Finally, Laser Metal Deposition (LMD**)**, also known as Laser Engineered Net Shaping (LENS), Direct Metal Deposition (DMD) or laser cladding, is a process in which the powder is completely melted by a laser beam, achieving a fully dense part without the need of post processing. The main difference between SLM and LMD is the powder material provision. In LMD the powder material is locally supplied by a powder feeding nozzle (Figure 2.3). This deposition method makes the process attractive for part repair and wear corrosion protection applications, since the set up preparation is largely reduced compared to SLM. The surface roughness in powder based processes depend on several variables, such as: material, powder grain size, geometry of final product and machine characteristics.

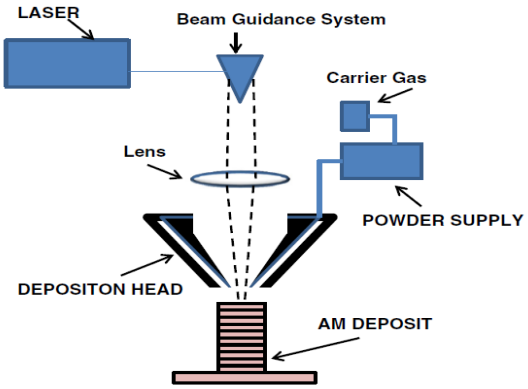

Figure 2.3 Generic illustration of a powder feed system [12]

According to the energy source, the wire-feed AM (Figure 2.4) can be classified into three groups, namely based on: laser, arc welding and electron beam.

Laser based technology has been the most popular due to its very good precision. However, laser has limited energy efficiency. When an electron beam is used as heat source a high vacuum environment is required, but this makes the setup time and costs higher than most processes, making the overall process efficiency and cost to fall. Compared to laser and electron beam, the arc welding processes, such as, metal inert gas/metal active gas (MIG/MAG) or tungsten inert gas(TIG), have a high energy efficiency which can be as high as 90% in some cases [5] and so, they have been investigated for this purpose.

Wire and Arc Additive Manufacturing (WAAM) is the designation given to the process that use an electric arc as a heat source. The Wire and Laser Additive Manufacturing (WLAM) is very similar to WAAM but the heat source is a laser beam instead of an electric arc. Other equipment, such as wire feed stock machine, shielding gas system and moving control system are still needed. In WAAM and WLAM special attention has been given to Ti-based alloys due to its intensive use in aeronautic industry [13-15].

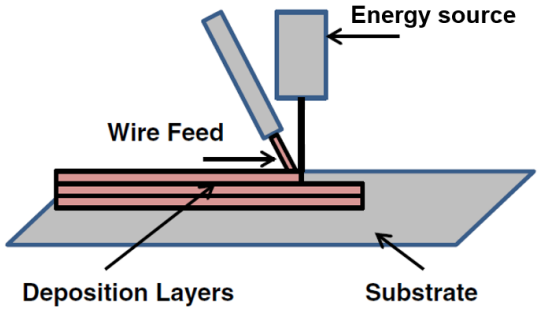

Figure 2.4 Schematic illustration of a wire feed based process (Adapted from [12])

Parameters such as, surface roughness, layer thickness and deposition rate are commonly used to characterize the AM processes. Typical values are presented in Table 2.3.

Table 2.3 Comparison of AM processes characteristic and processed materials

Process	Characteristics				Refs.
	Surface Roughness [μm]	Layer Thickness [μm]	Deposition Rate	Materials	
Selective Laser Sintering	~7-15	30-120	5-20 cm^3/h	Alumina, silica, zirconia, ZrB2, bioceramic, graphite, bronze-nickel	[2, 10, 16, 18-20]
Selective Laser Melting	~8-20	50	76 cm^3/h	Stainless steel GP1, PH1 and 17-4, cobalt chrome MP1, titanium Ti6Al4V, IN718, maraging steel MS1, AlSi20Mg, copper, Aluminium	[2, 6, 10, 21-24]
Electron Beam Melting	~46	70	80 cm^3/h	Ti6Al4V, Ti6Al4V ELI, cobalt chrome	[2, 25]
Laser Metal Deposition	~31-60	300-400	240 cm^3/h	Steel H13, 17-4 PH, PH 13-8 Mo, 304, 316 and 420, aluminium 4047, titanium TiCP, Ti-6-4, Ti-6-2-4-2 and Ti6-2-4-6, IN625, IN617, Cu-Ni alloy, cobalt satellite 21	[2, 17, 25]
Wire and Laser Additive Manufacturing	<50	N.A.	250 cm^3/h	Ti6Al4V, Fe-based and Al-based alloys	[5, 13]
Wire and Arc Additive Manufacturing	>180	N.A.	320 cm^3/h	Ti6Al4V, ER70S-6, ER4043, Ni6082, YS308L	[26-30]

2.3 Wire feed and Arc Additive Manufacturing

Wire-feed additive manufacturing is a promising technology for producing larger components with moderate complexity due to its high deposition rate. However, there are several issues that need to be improved such as: residual stresses and distortion from excessive heat input, relatively poor part accuracy and poor surface finish of the produced parts.

WAAM currently uses MIG or TIG equipment attached to a motion system that ensures the travel speed (TS), the direction and the contact tip working distance of the torch. MIG/MAG is a welding process in which an electric arc forms between a consumable wire electrode and the workpiece. TIG

uses a non-consumable tungsten electrode to create the electric arc. In order to protect the welding pool from the atmospheric environment a shielding gas is used in both processes. This gas can also help to improve the stability of the electrical arc. Metal inert gas (MIG) and Metal Active Gas (MAG) are both gas welding processes, being the shielding gas the main difference.

MIG is a suitable process for almost any metallic material, specially for reactive alloys that require inert atmosphere. Additionally, MIG has higher deposition rate when compared to MAG. Due to these factors, MIG is the most chosen process for WAAM.

One of the major issued in AM is the path planning method, that can highly affect the time to produce a part, especially when more than one feeding system is used.

In order to improve the material deposition efficiency (defined as the ratio of the real area of the geometry to the deposited area), Ding et al. [31] created an algorithm based on medial axis transformation, which can increase 2.4 times the material deposition efficiency. Recently, the same authors studied the influence of the welding parameters in the geometry of one single bead and used the results to build a software that get together all the steps of WAAM, from the CAD model to the finished part. They also developed a software to predict the deposited bead width and height, considering as input the welding parameters [32]. Several other authors have given attention to the bead modelling in order to optimize the bead overlapping and control the bead geometry [33–36] [37].

In a preliminary study Zhang et al. [38] developed a dedicated control technology for WAAM in which is included the CAD model processing into vector-based programing, path planning strategy and the control of deposition process parameters. A special control of the parameters has been given to both start and end of each pass where has been identified a higher and lower height, respectively. This phenomenon has been explained by the high heat sink at the beginning of the deposition that decreases the penetration and, consequently, increases the thickness of the layer. Opposite, at the end of the layer the higher temperature of the material promotes a lower heat dissipation and the height decreases. The problem has been solved by decreasing the travel speed and the current at the initial stage of the weld pass and increasing at the end, as shown in Figure 2.5.

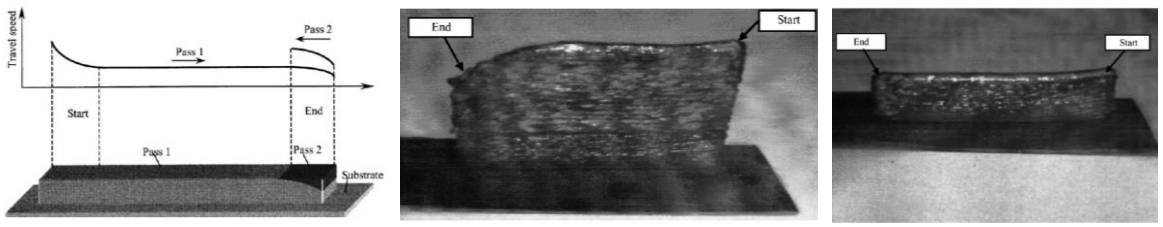

(a) (b) (c)

Figure 2.5 Influence of the TS control method. (a) TS control method for each pass, (b) non controlled deposition, (c) controlled deposition. [38]

In order to overcome the surface finish and accuracy problems of WAAM process, Song et al. [28] developed a mechanism based on a 3-axis milling machine with two welding guns that are vertically attached to the spindle housing. The two welding guns allow switching between two different wire materials or between two different wire material sizes, and a milling tool allowing subsequent surface finishing in the same setup [29].

In a similar study, which combine machining and MIG/MAG welding Akula et al. [39] developed a software to calculate the required adaptive slice thickness for the deposition of the filler metal and generate the required numerical control codes for machining.

Most of the studies in WAAM have been focused on the production of vertical thin walls, although this can cause accessibility problems and may require that the part is moved during the deposition process. Kazanas et al. [27] investigated the production of geometrical features using wire and arc additive manufacture with positional welding (Figure 2.6). Oblique and horizontal wall features have been built using an inclined torch position. Additionally, the effect of travel speed in the surface waviness has been investigated to better understand the effect on part quality for angled walls.

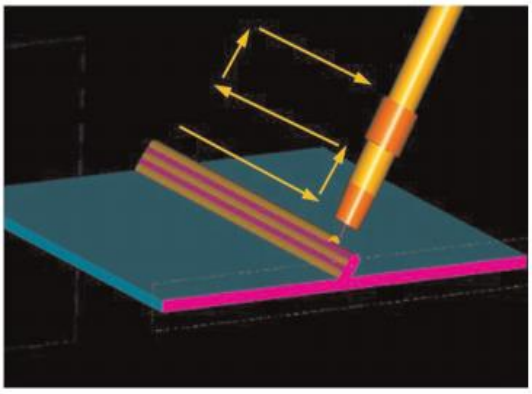

Figure 2.6 Inclined wall fabrication [27]

The WAAM processes opened a new range of production possibilities, even to produce in-situ alloys. It is possible to produce an alloy by depositing simultaneously different consumable wires with multiple welding torches. The alloy composition can be adjusted by controlling the WFS of both torches.

Shen et al. [40] produced an iron-rich Fe–Al intermetallic alloy in a thin wall shape. Using the TIG process with argon as welding shielding gas and two consumable wires, ø 0.9 mm 1080 aluminium wire and ø 0.9 mm black annealed iron wire. The results show the feasibility to produce the alloy with WAAM. The component exhibited consistent composition and full density, and a yield strength 50 MPa higher than the comparable material manufactured by conventional methods, although the elongation has decreased 0.5%.

Two welding torches have also been incorporated in a numerical controlled machine allowing to deposit two different materials in the same build part. In this experiment they have deposited a nickel-based (Ni6082) alloy over stainless steel (YS308L) previously deposited. No welding defects have been founded and the mechanical tests results show properties similar to the raw material. However the surface roughness measured was of 3 mm [26].

Haselhuhn et al. [41], studied various substrate release mechanisms that allow WAAM parts to be removed from a reusable print substrate with minimal energy. ER4043 aluminium and ER70S-6 steel wires were used as consumable materials. Aluminium oxide, boron nitride, and titanium nitride coatings were evaluated as possible substrate release agents for aluminium parts.

Table 2.4 summarises existing work on WAAM considering the technology, the process parameters and the materials used.

Table 2.4 Summary of WAAM in literature

Technology	Process parameters		Waviness	Material	Ref.
MIG	U=19 V; I=120 A; TS =1.2 m/min WSG - CO2 to Ar 30:70		150 µm	AWS 5.18 ER70S-6	[28, 29]
CMT	Steel	Aluminium	200-900 µm	ER70S-6 ER4043	[27]
	TS=1.5 m/min WFS=6m/min WSG - CO2 to Ar 20:80	TS=0.5 m/min; WFS=3.7 m/min WSG - 99.998 % Ar and He to Ar 25:75			
	GFR = 15 l/min	GFR = 16 l/min			
TIG	Aluminium WFS =0.7 m/min	Iron WFS =1 m/min	1 mm	99.5% black annealed iron 1080 aluminium	[40]
	U=12.7 V; I=140 A; TS =0.1 m/min				
MIG	Stainless steel	Nickel-based alloy	3 mm	Ni6082 YS308L	[26]
	U=20 V; I=80 A	U=20 V; I=80 A			
	WFS= 300mm/min; WSG- Ar to O2 98:2	WFS= 400 mm/min WSG 100% Ar			
	GFR = 15 l/min	GFR = 20 l/min			

2.4 Metal Inert Gas/Metal Active Gas

In MIG/MAG the processing parameters that can be controlled are: type of current, current intensity (I), voltage (U), wire feed speed, travel speed, electrode extension, wire diameter, welding shielding gas (WSG) and torch angle. Depending on the base material, electrode material, and weld characteristics desired, the parameters must be adjusted. The effect of process variable on weld attributes are presented in Table 2.5.

In order to create an electric arc, the major influent parameters are the current and voltage, the recent welding machines have pre-sets that automatically control the voltage and current values.

Table 2.5 Effect of changes in process variables on weld attributes

Parameters	Bead width		Penetration		Bead size		Deposition rate	
	Increase	Decrease	Increase	Decrease	Increase	Decrease	Increase	Decrease
Current and wire feed speed	↑	↓	↑	↓	↑	↓	↑	↓
Voltage	↑	↓	No effect	No effect	Small effect	Small effect	Small effect	Small effect
Travel speed	↓	↑	↓	↑	↓	↑	Small effect	Small effect
Electrode extension	↓	↑	↓	↑	↑	↓	↑	↓
Wire diameter	Small effect	Small effect	↓	↑	Small effect	Small effect	↓	↑
Shielding gas	↑	↓	↑	↓	Small effect	Small effect	Small effect	Small effect

Sometimes, thin materials can be a problem in welding, since arc forces can cut through, rather than weld. In addition, high deposition rates can result in a weld pool size that cannot be supported by surface tension in the vertical and overhead positions. However, the thickness and position limitations of spray transfer have been largely overcome by specially designed power supplies. These machines produce carefully controlled current outputs that "pulse" the welding current from levels below the transition current to above this [42]. They also allow lower heat input, which in WAAM is very important, leading to a lower dilution of the previous deposited layer and thus, to less extent heat affected zone (HAZ) and, consequently less grain coalescence and recrystallization.

In MAG four main metal transfer modes exist, which are: short-circuiting, pulsed arc, globular and spray (Figure 2.7). The drop transfer mode is a function of several factors, including current level, wire diameter, arc length, voltage level, specific power supply characteristics and shielding gas.

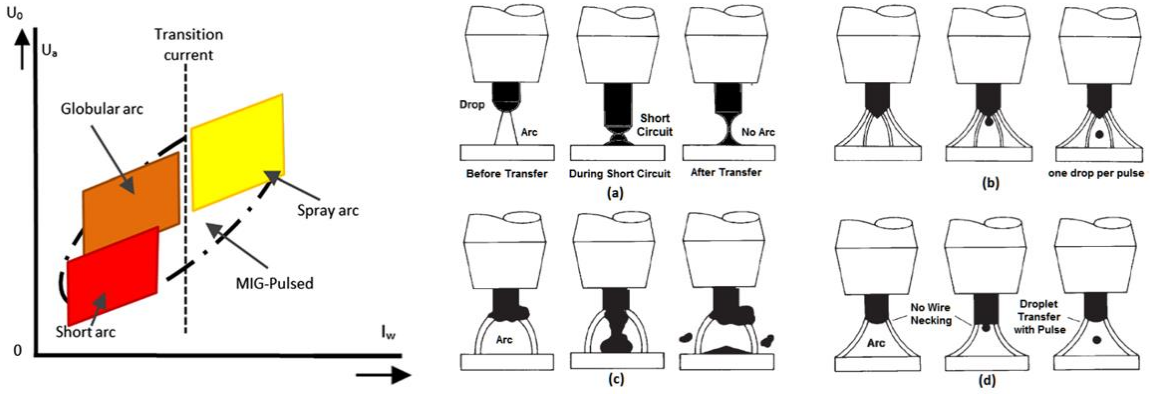

Figure 2.7 Transfer mode depicted in arc current and voltage, and drop transfer mode illustration. (a) Short-circuiting, (b) Pulsed, (c) Globular and (d) Spray [43,44]

Globular transfer mode is often considered the most undesirable one. It occurs when the current is relatively high, regardless of the type of shielding gas. However, the use of carbon dioxide or helium as main component benefits this type of transfer at all usable welding current range [42]. Globular transfer is characterized by a drop size with a diameter that is greater than that of the electrode with low detach frequencies, resulting in low productivity. The metal is transferred from the electrode to the base material only during the short-circuit time, when the electrode contacts the weld pool (Figure 2.8). The main electrode forces acting in the droplet detachment are the pinching force and the anode reacting force [45]. Usually, this transfer mode produces irregular weld beads with high spatter formation, but if the arc length is reduced the process can be stabilized and the spatter formation reduced [43].

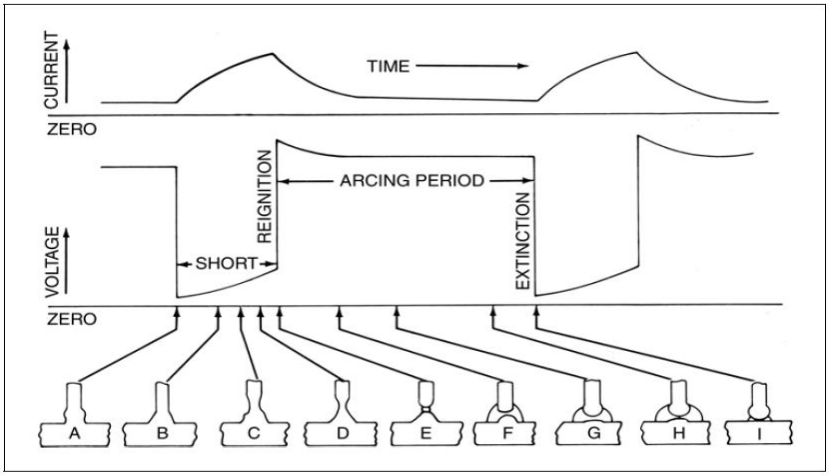

Figure 2.8 Cycle duty of short-circuit transfer [46]

Short circuiting transfer in IMG/MAG is determined by low arc current and voltage and consequently low heat input, making it suitable for weld thin parts. In this metal transfer, molten droplets are formed at the tip of the electrode but, instead of dropping to the weld pool when their critical size is reached, they bridge the gap between the electrode and the weld pool as a consequence of unsufficient arc length. This causes a short-circuit, which tends to extinguish the arc, that is quickly reignited after the surface tension of the weld pool pulls the molten metal bead off the electrode tip. In electrical terms, voltage and current oscillate between highs and lows (one inverted to the other) at the same frequency of the metal transfer. This type of metal transfer provides better weld quality and less spatter than the globular mode [44].

With a current level above the transition current and Argon shielding gas, it is possible to achieve the spray transfer mode. This is characterized by small droplets transferred between the electrode and the work piece, which are detached at a high-frequency as a result of high average current that creates high electromagnetic forces. High-quality weld finish and high production is obtained [44-47].

In pulsed arc transfer mode, it is possible to obtain a sequence of small droplets detaching in a very regular form, like in spray mode. This is reached by pulsing the current at a calculated frequency and duration, above a transition current. The high current peak detaches droplets of metal and the low current maintains the arc (Figure 2.9) [48]. The advantage of this transfer mode is the regularity and the low heat input, since the average current level is below the normal transition current [44].

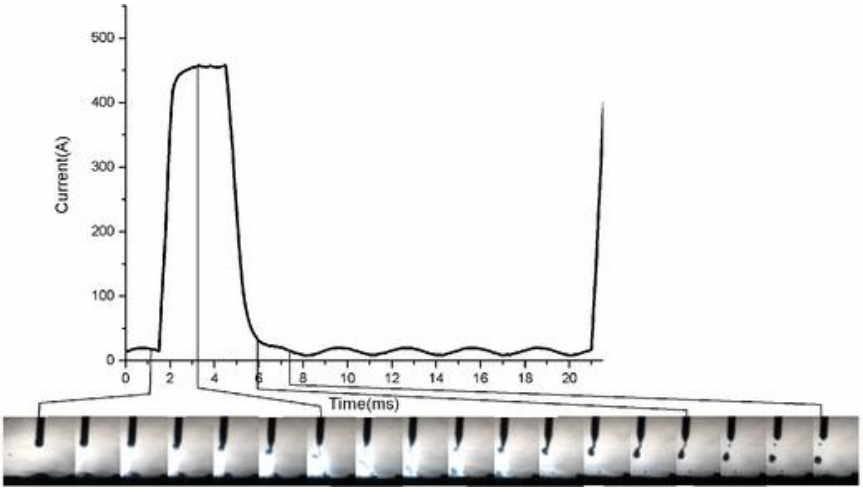

Figure 2.9 Example of welding current waveform and droplet in pulsed transfer mode [49]

The welding shielding gas major function is the protection of the welding pool from the atmospheric environment. However, its composition influences the material transfer mode, bead geometry, arc stability, weld appearance and welding speed [50].

The ionization potential is the energy, expressed in electron volts, necessary to remove an electron from a gas atom making it an ion, or an electrically charged gas atom. Gases with low ionization potential, such as argon, can change atoms into ions easily and, consequently, create a stable electric arc with an easier start. Thermal conductivity of the shielding gas influences the radial heat transfer from the centre to the periphery of the arc column as well as the heat transfer between the plasma and the weld pool. Low thermal conductivity gases produce an arc with a narrow hot core and a cooler outer zone, and a weld bead with a narrow root and wider top. Gases with high thermal conductivity, as helium, produce wider arcs, enhancing the penetration characteristics, allowing faster travel speed and higher productivity rates. Table 2.6 shows the ionization potential and thermal conductivity of the gases used throughout the work.

Helium is often added to argon in binary mixtures. He increases the penetration of the weld pool, due to the hotter arc produced. Both argon and helium are inert gases, but active gases such as carbon dioxide and oxygen are common mixed with inert gas. Small additions of oxygen (3-5%) or carbon dioxide (up to 20%), which allows spray transfer mode, improve the arc stability, humidity and the weld quality [42]. Additionally, He is a good heat extractor which promotes high cooling rates.

Carbon dioxide is the only reactive gas suitable for use alone as shielding gas in MAG. High travel speeds and deep penetration associated with its low costs are the characteristics that have promoted the use of pure CO_2 as shielding gas. However, the spatter formation increase and the metal transfer mode is limited to short-circuit or globular. Axial spray transfer requires an argon shield. Active gas reacts with elements in the filler metal or in the base plate and forms a slag on the surface. The loss of elements can affect the quality and mechanical properties of the weld [46].

Mixtures of Argon-Helium-Carbon Dioxide, where argon is the primary constituent, are used in pulsed-current welding of carbon and low-alloy steel. This mixture improves wetting and puddle fluidity, and allows a good spray transfer mode [42].

Table 2.6 Ionization potential and thermal conductivity of shielding gases

Gas	Ionization potential (eV) [42]	Thermal conductivity (W mm^{-1} K^{-1}) [51]
Argon (Ar)	15.7	17.74
Helium (He)	24.5	155.9
Carbone dioxide (CO_2)	14.4	16.85

2.5 Conclusion remarks

The additive manufacturing brought a wide range of new production possibilities for a large variety of industries. The special interest revealed by the aeronautic industry has contributed to the metal AM rapid development.

Among the various AM processes that use metallic materials, SLS, SLM and LDM are the processes that have been mostly studied.

At the present, WAAM is very attractive when compared with other AM processes for metals, due to its higher deposition rate and the capability to produce larger components. Also, it does not require specific equipment which implies lower capital investment. However, limited studies still exist. In terms of materials the ER70S-6 mild steel and Ti-based alloys are the most used.

This work contributes to the state-of-the-art of WAAM by studying the viability to use a new material, a low alloy high strength steel.

3

Experimental procedure

This chapter describes the materials, welding consumables and equipment used throughout this work, as well as, modifications introduced in the source and moving system for the set up preparation and data acquisition system. The experimental approach and characterization techniques are detailed.

3.1 Materials

The material used as a substrate for the depositions was a structural steel plate with 200x100x10 mm dimensions.

Two types of solid wire consumable electrodes were used to perform the deposition, both with 1 mm diameter. In the preliminary tests, AWS A5.18 ER70S-6 mild steel solid wire was used to estimate the best range of processing parameters and, in a further stage, a low alloy high strength steel AWS A5.28 ER110S-G. For both wires, carbon equivalent and maximum hardness were calculated according to empiric equations (1) and (2), respectively, in order to assess their hardenability and weldability problems due to weld thermal cycles [52].

$$C_{eq\,(\%)} = C + \frac{Si}{25} + \frac{Mn + Cu}{16} + \frac{Cr + Ni}{20} + \frac{Mo}{40} + \frac{V}{15} \tag{3.1}$$

$$HV_{max} = 90 + 109\,C + 47\,Si + 75\,Mn + 30\,Ni + 31\,Cr \tag{3.2}$$

Table 3.1 summarizes the chemical composition and mechanical properties of deposited material for both consumables, as well as, the carbon equivalent and maximum hardness Vickers.

Commercial pure argon and argon-helium-carbon dioxide mixture were used as shielding gases. Table 3.2 shows the chemical composition of these.

Table 3.1 Chemical composition and mechanical properties of the deposited material

Chemical composition (wt.%) [53]

	C	Mn	Si	Ni	Cr	Mo	V	Cu	Fe	$C_{eq\ (\%)}$
ER70S-6	0.09	1.60	0.84	<0.04	0.03	<0.01	<0.01	0.20	Balance	0.24
ER110S-G	0.08	1.70	0.44	1.35	0.23	0.30	0.08	0.25	Balance	0.31

Mechanical properties of deposited material [53]

	Yield Strength (N/mm^2)	Tensile Strength (N/mm^2)	Elongation (%)	Impact ISO-V (J) -40°C	HV_{max}
ER70S-6	400	485	22	N.A	261
ER110S-G	710	790	20	70	295

Table 3.2 Shielding gas compositions

Arcal 121	Ar	He		Carbon dioxide
	79 - 85%	16 - 20%		1 – 5%
Alphagaz 1	Ar	H_2O	O_2	C_nH_m
	99.999 %	<3 ppm	<2 ppm	<0.5 ppm

3.2 Equipment

3.2.1 Welding and motion equipment

A welding machine from *KEMPY* , model *Pro MIG 501* (wire feeder and control unit) and model *Pro MIG 3200* power source, were used to deposit the material over the substrate (Figure 3.1-(a)).

In order to remotely control the torch trigger, the machine was modified by adding an electrical bypass to the torch trigger, connected to an ON/OFF switch (Figure 3.1-(c)). This machine allows 3 MIG welding options, namely synergic pulsed wave, synergic continuous wave and conventional continuous wave. In synergic mode the WFS can be fully selected, but the current and voltage waves only may be slightly adjusted. In the conventional continuous wave mode it allows to set the voltage value independently of the WFS value.

(a) (b) (c)

Figure 3.1 Welding equipment. Wire feeder and power source (a), control panel (b), remote switch (c).

3.2.2 Electrical data acquisition

In order to obtain more precise values of the voltage and current intensity than those provided by the welding equipment, an instrumentation setup was designed and built. Both voltage and current intensity data were recorded using *National Instruments USB 6008* data acquisition system and a *LabVIEW* software.

For the current data acquisition a *LEM LA 200-P* current probe was placed in the ground cable and connected to a circuit that allows the user to know the current in the system by reading the voltage value in a resistor series connected to the current probe (Figure 3.2).

The data acquisition system only allowed to use voltages between -10 and 10 V. Due to this limitation an electrical voltage reducer circuit has been built (Figure 3.2) with an attenuation ratio of 31, calculated according to following equation.

$$\frac{\Delta U_1}{R_{eq}} = \frac{\Delta U_2}{R_2} <=> \frac{\Delta U_1}{\Delta U_2} = \frac{R_{eq}}{R_2} = \frac{3052.07}{98.47} = 31 \quad (3.3)$$

In both current and voltage data acquisition the rate of the measurements was 2000 measurements/second.

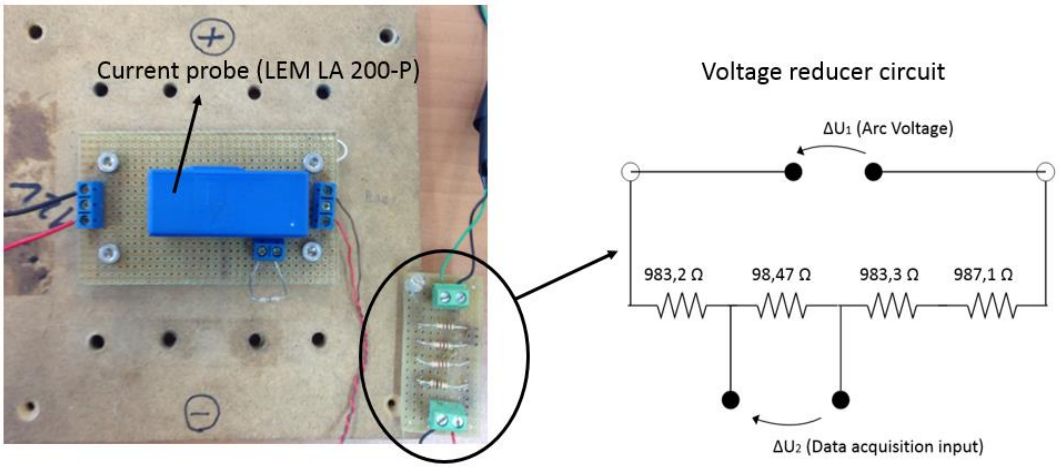

Figure 3.2 LEM LA 200-P current probe and voltage reducer circuit.

To obtain the arc voltage drop, the input of the voltage reducer circuit was connected to the welding torch and to the substrate material. In order to get a precise value of the arc voltage drop, the connection at the torch was placed as near as possible of the torch nozzle, taking into account the high temperature at that position. This allows eliminating the error introduced by the voltage drop in the elements that conduct the current to the nozzle. Figure 3.3 shows the connection of the voltage reducer circuit to the torch (green wire) and to the substrate material (black wire with a crocodile clamp). The data saved in text file was then processed in *MatLab* to calculate the voltage and current intensity, as well as, the root mean square.

Figure 3.3 Connection of the voltage reducer circuit to the torch and substrate material

3.2.3 Motion system

In order to guarantee repeatability of the deposition conditions and parameters, a workstation with a one-axis moving table was used (Figure 3.4). The travel speed was controlled by *GW Instek: GFG-8020 M Function Generator* (wave generator). Additionally, a program in *LabVIEW* was developed to control the deposition distance. The torch holder was modified to improve the clamping device and also to control the contact tip to work distance (CTWD) with a threaded spindle rod system (Figure 3.5).

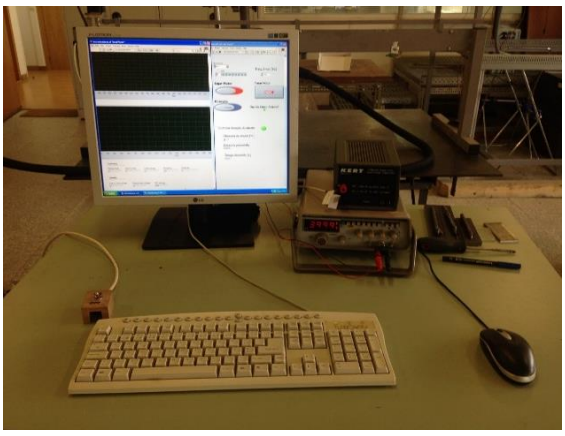

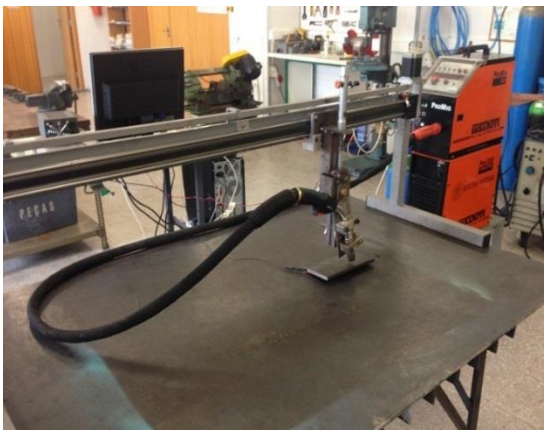

Figure 3.4 Experimental apparatus

Figure 3.5 Torch clamping and height control

3.3 Build-up strategy

The path performed by the welding torch influences the thermal gradient, the solidification conditions and the residual stresses generated. In order to obtain a similar thermal gradient and a cooling rate along the specimen, it was made a one-direction deposition, as illustrated in Figure 3.6. The green lines represent the deposition path, and the red lines the torch movement without deposition.

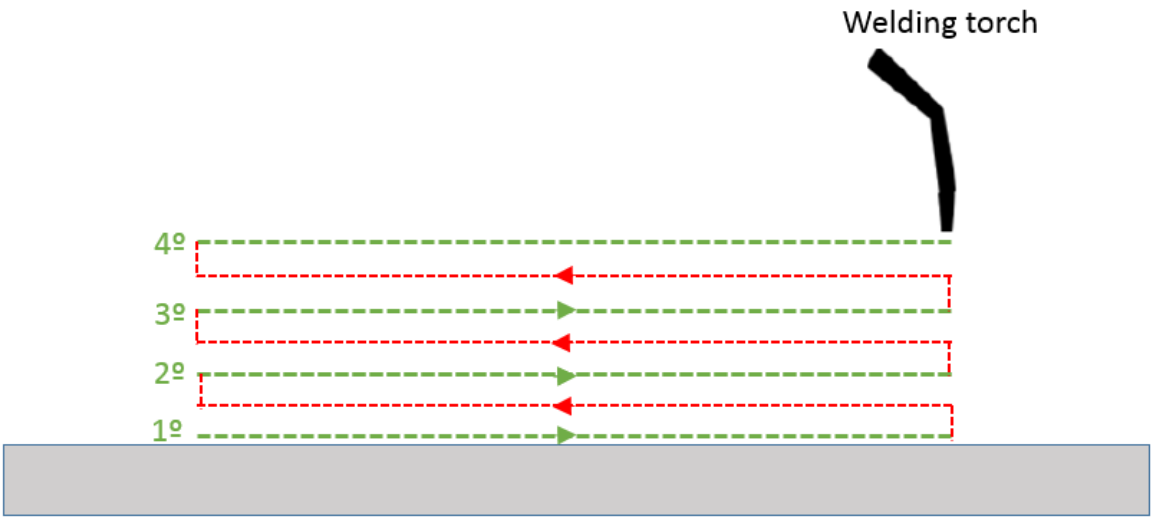

Figure 3.6 Deposition path

3.4 Heat input and deposition rate calculation

From the acquired data, the heat input was calculated according to eq. 3.3.

$$HI = \frac{U \times I}{TS} \times \eta \qquad (\mathrm{J/mm}) \qquad (3.4)$$

where U is the RMS voltage (V), I the RMS current (A) and TS the travel speed (mm/s). The efficiency of the MIG welding process was considered 0.8.

The deposition rate was calculated from geometrical features measured using eq. 3.4.

$$DR = \frac{L \times W \times H}{DT} \qquad (\mathrm{cm^3/h}) \qquad (3.5)$$

where L is the deposition length (cm), W and H the average width and height (cm) and DT the deposition time (h).

3.5 Characterization techniques

3.5.1 Sample preparation

Each sample was evaluated by several characterization techniques. Two different types of preparation were performed, one for optical microscopy observations and the other for the uniaxial tensile tests. For the microscopic observation a 'slice' was cut from the deposition performed, the back plate was removed and finally embedded in resin as illustrated on Figure 3.7. The samples for uniaxial tensile test were obtained from a section of the parts produced as shown in Figure 3.7 and produced in a MELDAS VMC 50 machining centre.

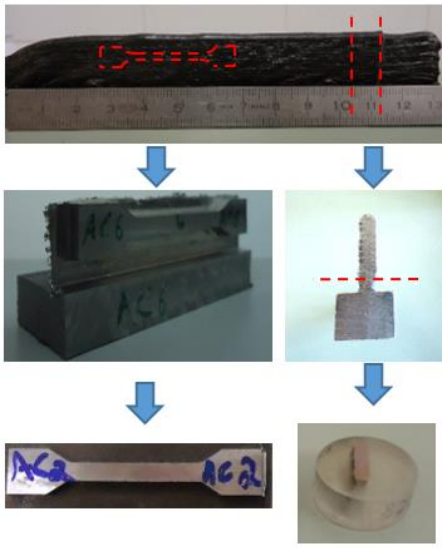

Figure 3.7 Sample preparation

3.5.2 Optical microscopy

For microscopic observation the samples embedded in resin were grinded and polished with abrasive diamond 1 μm paste and chemically etched with Nital (2 % solution).

The microstructures were then examined and recorded using a *Leica* DMI 5000 M inverted geometry microscope.

3.5.3 Microhardness measurements

After the optical microscopy observation, Vickers microhardness measurements were performed, along a vertical line with a distance between each indentation of 0.15 mm in the center of the sample (Figure 3.8). The equipment used was a Mitutoyo HM-112 microhardness tester by applying a test load of 3 N during 10 seconds.

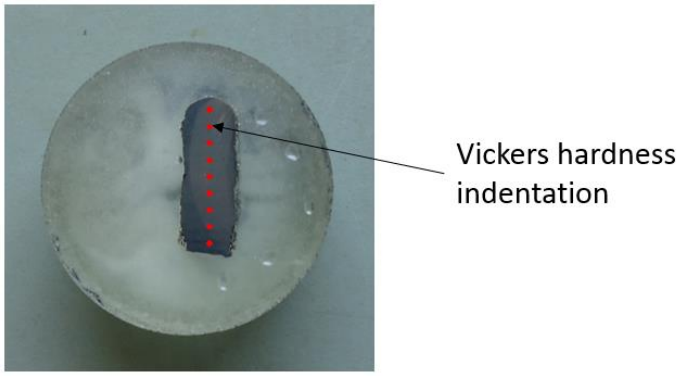

Figure 3.8 Schematic representation of Vickers hardness indentation

3.5.4 Uniaxial Tensile Tests

Uniaxial tensile tests were performed at room temperature, at CENIMAT, on an AUTOGRAPH SHIMADZU model AG500Kng equipped with a SHIMADZU load cell type SFL-50kN AG with a total capacity of 50 kN. Just one uniaxial tensile test specimen was possible to prepare from each sample due to the size of the produced part.

3.5.5 Scanning Electron Microscopy

Scanning electron microscopy (SEM) was used to analyse the homogeneity of the chemical composition of the part, as well as, the fracture surface of the uniaxial tensile test specimens.

An equipment from ZEISS DSM 962 ESM, available at CENIMAT was used. SEM was equipped with an energy dispersive X-ray spectrometry (EDS) from Oxford Instruments, INCA X-ACT. The acceleration voltage used was 20 kV at a magnification of 50x.

3.5.6 High Energy Materials Science beamline

XRD analysis was performed at DESY facilities (HEMS - High Energy Materials Science beamline) at PETRA III in Hamburg, Germany. It was used a wavelength of 0.1426 Å (87 keV). A 2D detector was used and the tests were held at room temperature (21 °C). Laser was kept in the path for the X-ray which allowed foreseeing where on the sample the X-ray beam would hit. By moving the vertical motion motors, remotely from the control room, alignment was performed by illuminating the deposited material in the specimen, with the laser beam. Scans were recorded successively in a vertical line of samples similar to the uniaxial tensile test specimens. The beam spot was of 0.1x0.1 mm. The exposure time was kept from 5 to 10 seconds.

3.6 Design of experiments

Since the number of processing parameters to consider was very high a design of experiments (DOE) was used to minimise the number of tests.

DOE is a systematic approach to experimentation, focused on the data collection stage, to determine the relationship between factors affecting a process and the corresponding output that has one or more observable responses. Taguchi method is an experimental design that uses statistical methods to analyse the process parameters, designated as factors, and indicate the most influents and how they affect the selected response [54]. Low and high levels of factors are commonly referred to as 1 and 2 [55]. Taguchi suggested the S/N ratio as a measure of quality characteristics deviating from or near to the desired values. In order to evaluate the significance of the parameters used in the process, analysis of variance (ANOVA) was applied in a statistical study of Taguchi's method. Analysis of variance is a statistical hypothesis testing whose purpose is to test for significant differences between means. The results of the analysis are presented in a table (ANOVA table) that determines the most relevant parameters for the process through the sources that contribute to the total variation in the data values.

In this study the design of experiments (DOE) was used in order to understand the influence of the process parameters in the built piece. Initially, two-level full factorial and half fraction factorial designs were considered, but with five factors, the number of experiments required was 32 (2^5) and 16 (2^{5-1}), respectively. Since producing this number of samples would require the use of many resources such as base material, welding consumables, and time, both full factorial and half fraction factorial were discarded and the Taguchi Method was chosen, which allows the reduction of experiments to 8. This allowed to fully understand the combined effects of these five parameters. As the number of tests is much more feasible it was decided to create two models according to the type of the current wave, which results in a total of 16 experiments.

Taguchi method based design of experiment has been used to study effect of five welding process parameters (GT, GFR, WFS, TS and U) on three major output parameters, namely average width, deposition rate and waviness. Following Taguchi's method, two experimental designs were selected with five variables each, the first for synergic pulsed wave and the other for continuous wave, as shown in Table 3.3. During the experimentation the CTWD of 4 mm and a torch angle of 80° were maintained constant.

The appropriate orthogonal arrays were selected according to the number of factors intended to analyse. Since the number of factors is five (N), the number of degrees of freedom is 4 (N-1) so Taguchi based L8 orthogonal array is selected. Accordingly, 8 experiments were carried out to study the effect of welding input parameters for each model. Table 3.4 shows the L8 orthogonal array designed based on the Taguchi method for both models.

Table 3.3 Factor levels for DOE

Synergic pulsed wave model			Continuous wave model		
Factors	Levels		Factors	Levels	
	1	2		1	2
Gas type (GT)	Arcal 121	Alphagaz 1	Shielding gas (SG)	Arcal 121	Alphagaz 1
Gas flow rate (GFR)	8 (l/min)	16 l/min	Shielding gas flow (SGF)	8 (l/min)	16 l/min
Wire feeding speed (WFS)	2.5 (m/min)	5.5 m/min	Wire feed speed (WFS)	3.0 (m/min)	5.0 m/min
Travel Speed (TS)	3.8 (mm/s)	9 mm/s	Travel Speed (TS)	3.8 (mm/s)	9 mm/s
Voltage adjustment (knob position)	-6	+6	Voltage (U)	21.0 (V)	26.0 (V)

Table 3.4 Taguchi L8 orthogonal array

	Factors Levels				
Run	SG	SGF	WFS	TS	U/VA
1	1	1	1	1	1
2	1	1	1	2	2
3	1	2	2	1	1
4	1	2	2	2	2
5	2	1	2	1	2
6	2	1	2	2	1
7	2	2	1	1	2
8	2	2	1	2	1

4

Results and discussion

4.1 Preliminary tests

A first set of experiments was conducted with a common consumable electrode, a low carbon steel one, ER70S-6, in order to set a suitable range of both wire feeding speed and welding speed. This electrode was chosen due to its wide availability and low costs. Since this electrode had the same diameter as the one to be studied in this work, it was a reasonable assumption.

Table 4.1 shows the processing parameters used in the preliminary tests and Figure 4.1 depicts the aspect of the deposits, as well as, the transversal section profile. Tests were performed at travel speeds of: 3.2, 7.3 and 11.5 mm/s, in pulsed mode.

Table 4.1 Processing parameters

	P1	P2	P3
Nº of layers	14	14	14
WFS (m/min)	3	3	3
SGF (l/min)	14.5	14.5	14.5
I (A)	78	75	77
U(V)	21.2	22.6	19.8

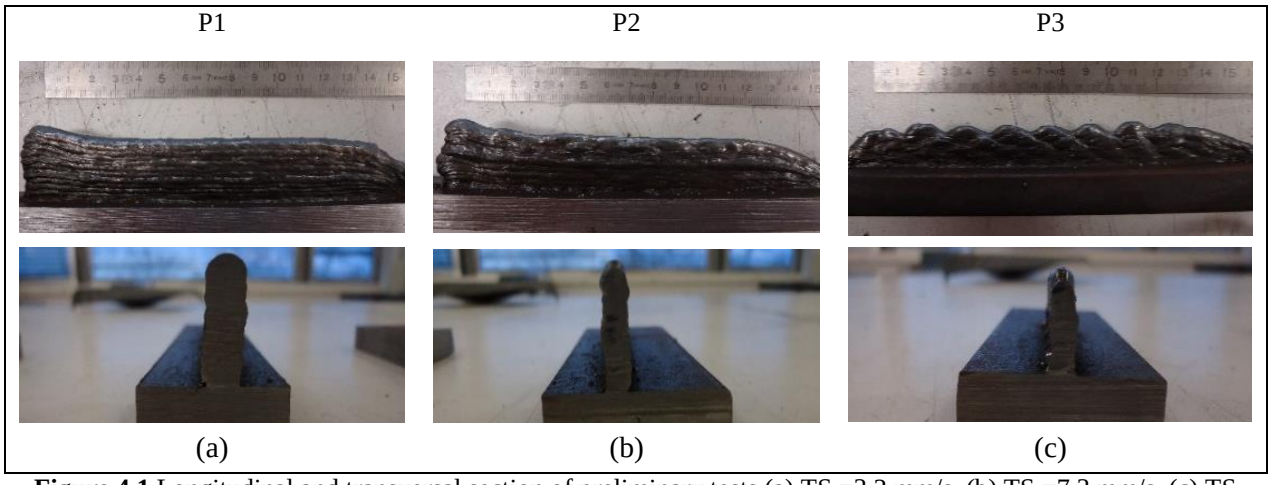

Figure 4.1 Longitudinal and transversal section of preliminary tests (a) TS =3.2 mm/s, (b) TS =7.3 mm/s, (c) TS =11.5 mm/s.

It is clear that a weld bead humping occurred at higher values of the travel speed. This effect is not perfectly understood [56] but seems to be due to the forces exerted by the drop in the interaction area leaving behind an undercut, thus forming a periodic undulation consisting of a hump and a valley. It was also observed that the defect is more protruding after successive layers, up to a point when the process becomes unfeasible.

In a second set of tests the influence of the WFS in the weld bead humping was analysed. The WFS values were defined as: 2, 2.5 and 3 m/min. Travel speed was set at 11.5 mm/s to verify the effect of WFS on the weld bead humping identified. All other parameters were kept constant and are depicted in Table 4.2.

Table 4.2 Fixed processing parameters as well as, voltage and current intensity values

	P4	P5	P6
Nº of Layers	14	14	14
TS (mm/s)	11.5	11.5	11.5
SGF (l/min)	12	12	12
I (A)	45	66	75
U(V)	20.1	21.3	26.9

It was seen that increasing the WFS, attenuated the weld bead humping (Figure 4.2), but the process was not stable. Increasing the WFS, the weld bead enlarged and became smoother. Thus, the TS was set between 3.2 and 9 mm/s in the subsequent experiments.

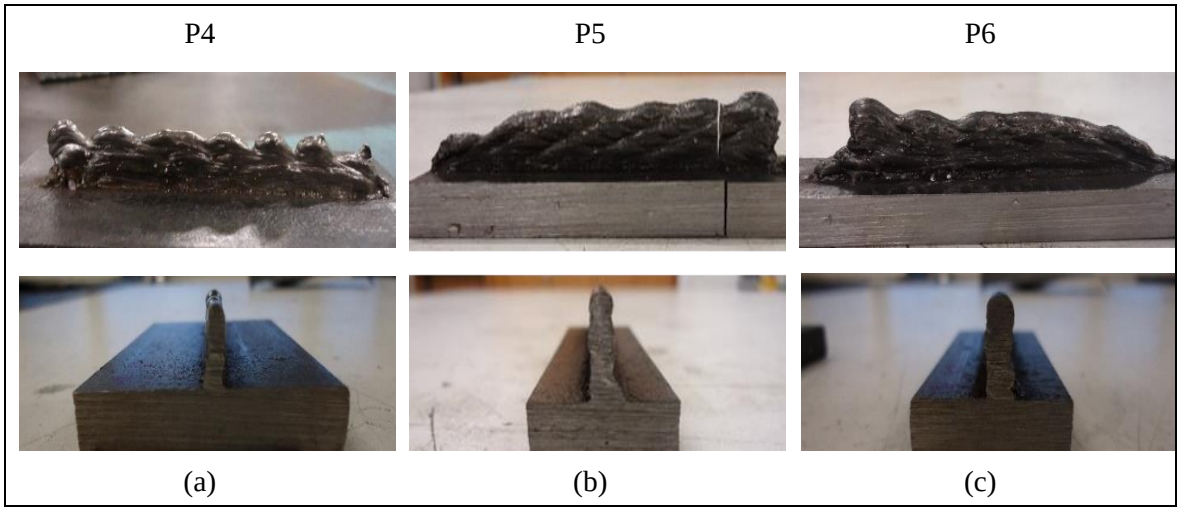

Figure 4.2 Preliminary tests (a) WFS =2 m/min, (b) 2.5 m/min, (c) 3 m/min

4.1.1 Effect of processing parameters on the deposit geometry

From the width and height measurements of the depositions presented in Table 4.3, it can be seen that both WFS and TS affect the weld bead profile as expected from conventional welding knowledge. This results are expressed graphically in Figure 4.3 to 4.6

Table 4.3 Average width, height per layer and waviness, and heat input of preliminary tests

	P1	P2	P3	P4	P5	P6
Height/ layers (mm)	1.36	1.21	0.71	0.75	0.86	0.85
Width (mm)	8	5.5	4.5	3.5	4	5.5
Waviness ($\mu m \pm \sigma$)	293.3±83.3	593.5±226.3	706.9±394.1	451.0±174.4	560.6±262.0	499.8±285.0
Heat input (J/mm)	414.7	184.8	106.2	63.0	97.9	140.5

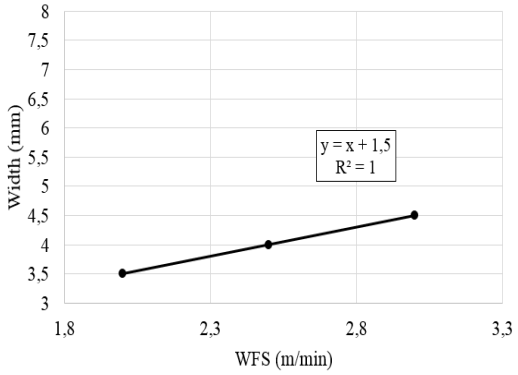

Figure 4.3 Effect of WFS on bead width

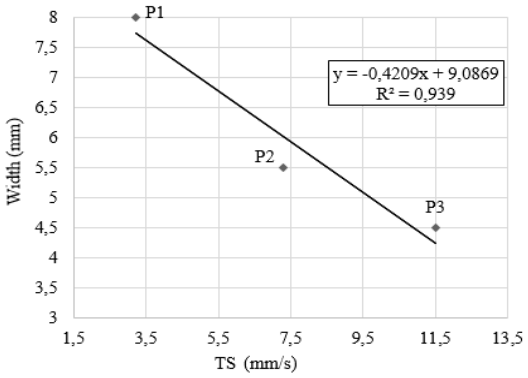

Figure 4.4 Effect of TS on bead width

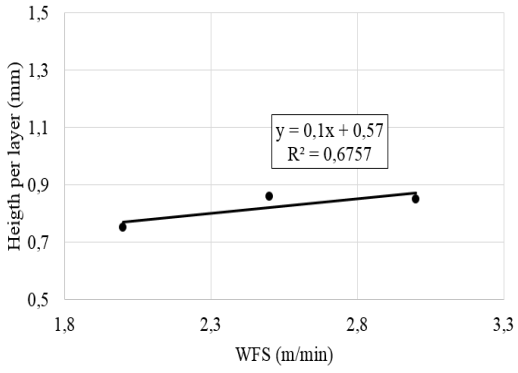

Figure 4.5 Effect of WFS on height per layer

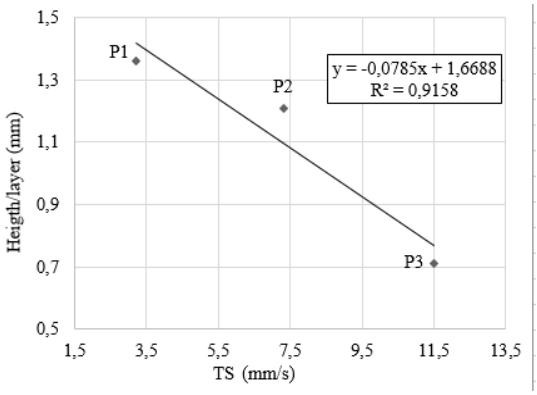

Figure 4.6 Effect of TS on height per layer

Analysing the figures, there is a clear trend on the effect of parameters on the average width and height per layer. Keeping all other parameters constant, an increase of WFS increase both the width and the height of each layer. The travel speed has the opposite effect, that is, when the travel speed decreases, the material deposited per unit of length increases and consequently the overall bead size increases.

Moreover, it can be observed that both TS and WFS have more influence in the width than in the height per layer by analysing the slope of the adjusted functions.

Increasing the heat input, the temperature of the molten material is higher and, thus, improve the wetting conditions, i.e. promotes a more fluid flow of the molten material, which leads to a flat weld bead with a larger width (Figure 4.7).

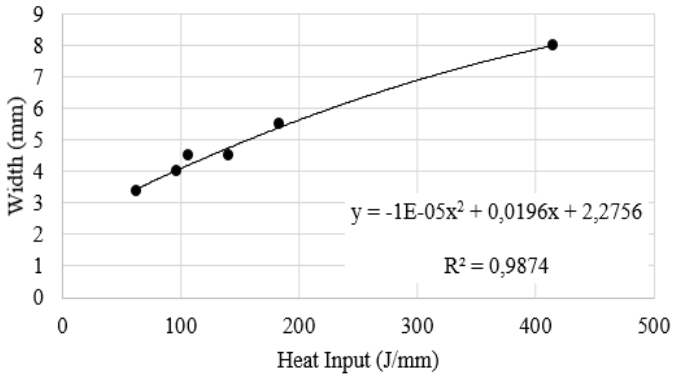

Figure 4.7 Effect of HI on bead width

4.1.1 Microhardness

The microhardness tests were performed in order to indirectly evaluate the ultimate tensile strength of the deposit. The measured values along the height of the depositions are depicted in the figures below, in which zero was set at the bottom of each sample.

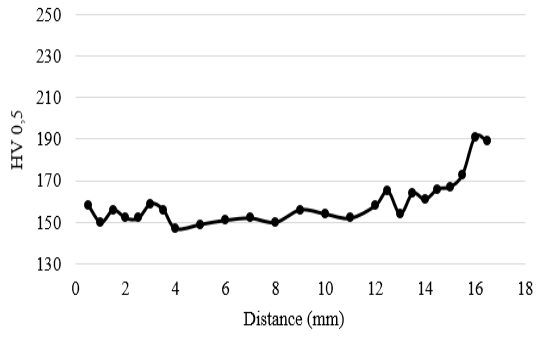

Figure 4.8 Hardness distribution along the section of P1 sample

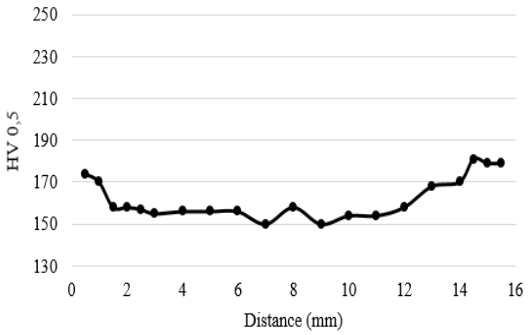

Figure 4.9 Hardness distribution along the section of P2 sample

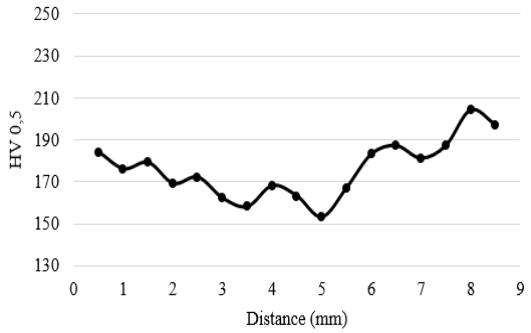

Figure 4.10 Hardness distribution along the section of P3 sample

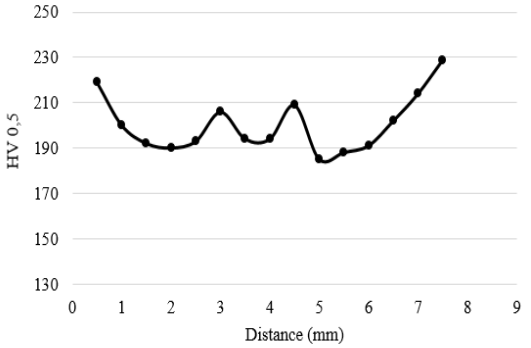

Figure 4.11 Hardness distribution along the section of P4 sample

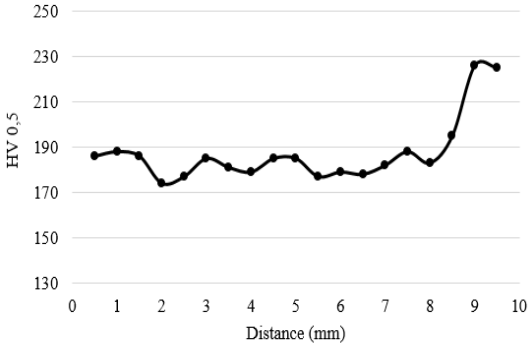

Figure 4.12 Hardness distribution along the section of P5 sample

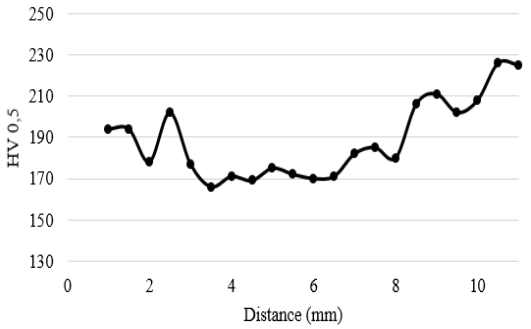

Figure 4.13 Hardness distribution along the section of P6 sample

In most of the samples the hardness is higher in the first and last layer deposited, that is, in the top and the bottom of the deposit. This was expected since these regions undergo the highest cooling rates: the first layer cools to the cold back plate, and the last one, rapidly cools in contact with shielding gas and atmosphere. The last layer, on the top of the deposit is not subjected to further thermal cycles, so there is no annealing effect.

4.1.2 Microstructure

Microscopic observations of the specimens revealed three distinct zones. Associated with the last layer deposited is an upper region, which corresponds to the fusion zone. Below this, is a gradient of microstructures where two different zones are identified: the heat affected zone (HAZ) of that layer and a re-melted zone (RZ) of the previously deposited layer (Figure 4.14).

In the fusion zone there is an epitaxial columnar grain structure, resulting from grain growth over pre-existing solid grains with a favourable crystallographic orientation perpendicular to isothermal curves, that is, parallel to heat flow direction. The same is observed in the partially re-melted zone. In the heat affected zone the structure depends on heat input, that is on the cooling rate and peak

temperature attained. Fully austenitic regions show pro-eutectoide ferrite along the austenite grain boundaries and ferrite and pearlite in the center. However, when the heat input is very low other transformation products of austenite can be seen as bainite due to the relatively low carbon content of the wire.

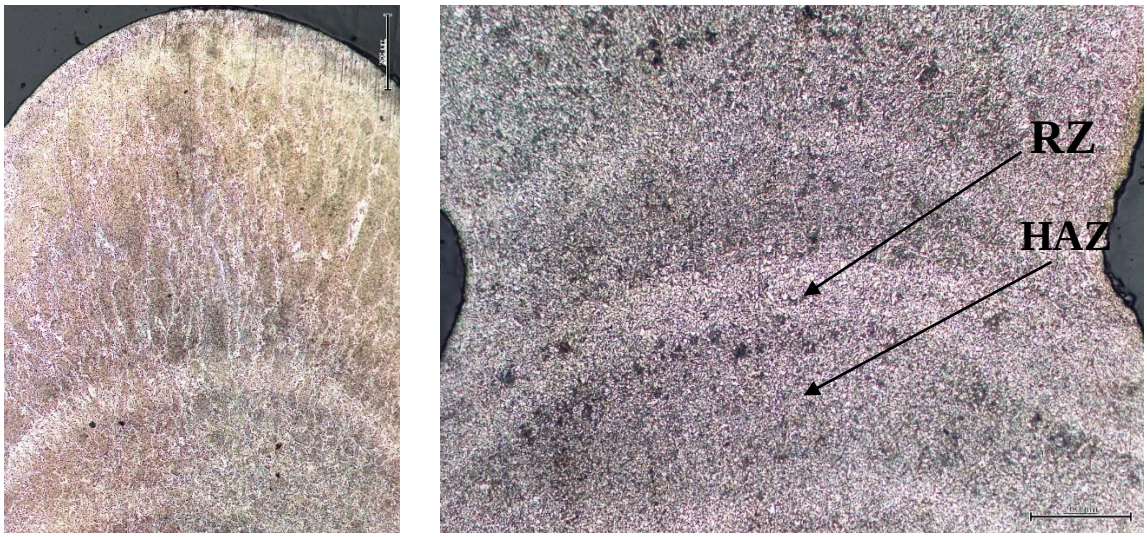

(a) (b)

Figure 4.14 Macrostructure of (a) top and (b) intermediate layer

Representative microstructures from the re-melted zone and heat affected zone from the centre of the specimens are shown in Figure 4.15 and 4.16**,** respectively.

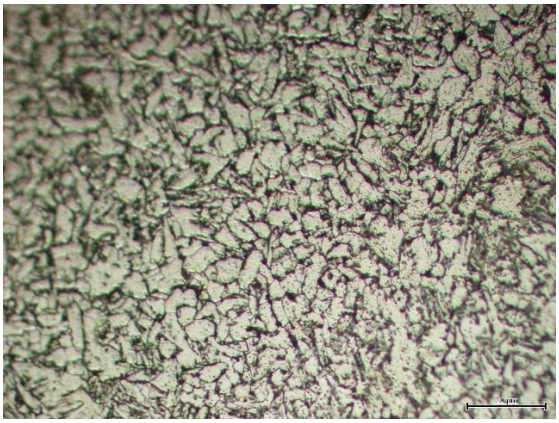

Figure 4.15 Microstructure of the RZ

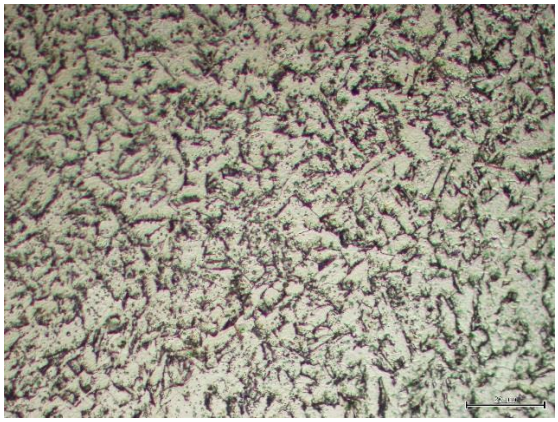

Figure 4.16 Microstructure of the HAZ

Under optical microscopy observations, some samples presented very small irregularities that were classified as pores. A quantification of these on sample P5, which had a more porous aspect, showed a maximum porosity of 0.34 %, which was considered not significant.

However, observing these cavities under SEM, it was seen a very fine dendritic structure inside the pores as shown in Figure 4.17. These structures are very fine, the cavities have less than 5 µm diameter and are quite surprising. Either they are developing from the solidified structure and have this aspect since the surface had not been etched, or some partial liquid remained in the interdendritic

spaces. Nevertheless, the magnitude of these dendritic structures is about the same as those observed on the facture surface of tensile specimens discussed later in this thesis. The presence of these pores deserves some attention but this is out of scope of the present study.

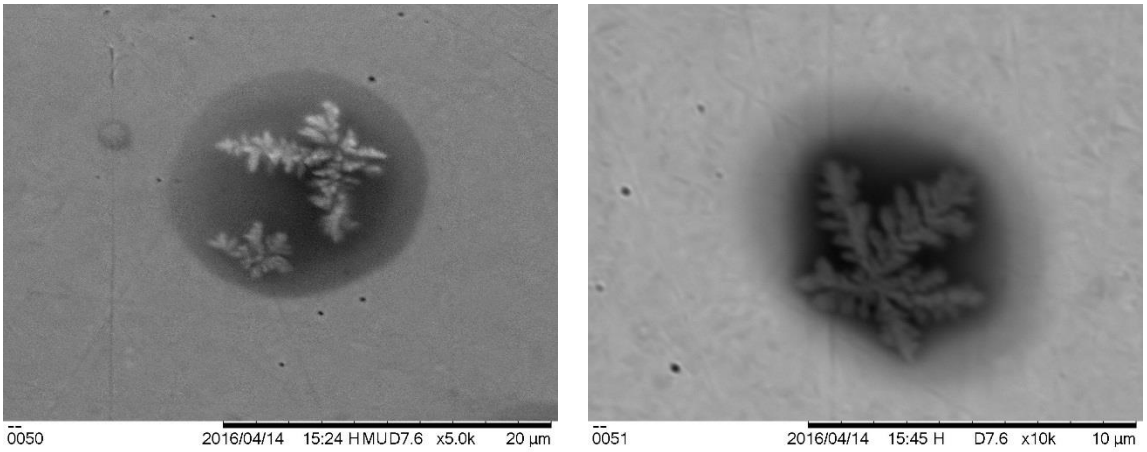

Figure 4.17 SEM observations of open pores

After these preliminary tests and the identification of the best range of parameters for deposition, these were considered when defining the DoE

4.2 Taguchi method results

For both pulsed wave mode and continues wave mode, the influence of gas type (GT), gas flow rate (GFR), wire feeding speed (WFS), travel speed (TS) and voltage (U) on average width, waviness and deposition rate was studied. Interactions between parameters and their effect on the output parameters was also analysed.

The red dashed lines represent ±2x standard deviation, relatively to the mean value for each response. The parameters which have an influence higher than 2x the standard deviation were considered the significant ones.

In the pulsed wave mode, it is clear that both WFS and TS are the most influent parameters (Figure 4.18), which confirm the preliminary tests results. The gas type influence on the width is almost negligible. An increase in gas flow rate causes a reduction of the width, as expected, since at high gas flow rates, the heat dissipation is more effective leading to higher cooling rates. So the deposition becomes thin. However, at high travel speeds the gas flow rate does not have the same effect due to the low interaction time of gas with the deposited material (Figure 4.20).

In continuous wave mode, the travel speed is the most influent parameter followed by the wire feeding speed and voltage, both with similar influences. The WFS directly affect the volume of deposited material, while the current intensity is also indirectly controlled by the WFS. Consequently, the heat input is affected by WFS, TS and current intensity.

It was seen in the preliminary tests that the HI had a direct influence on the width of the deposited layer, which is confirmed by the DoE analysis (Figure 4.19). Under similar conditions, continuous wave mode originate a higher heat input, that makes the gas flow rate effect on cooling rate less significant than in pulsed wave mode (Figure 4.21).

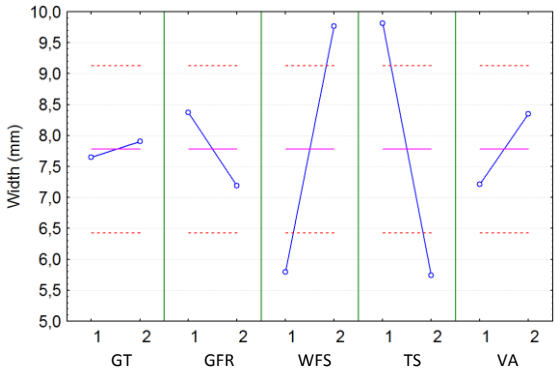

Figure 4.18 Effect of process parameters on width average in pulsed wave mode

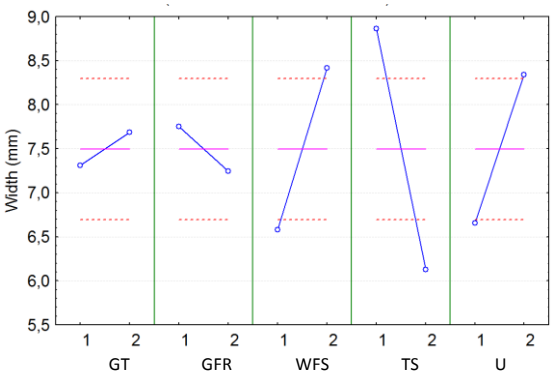

Figure 4.19 Effect of process parameters on width average in continuous wave mode

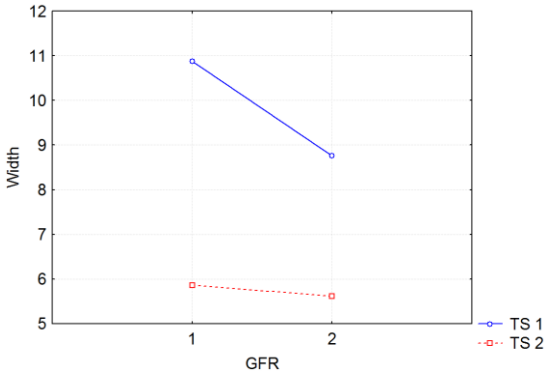

Figure 4.20 Interaction between GFR and TS in pulsed wave mode

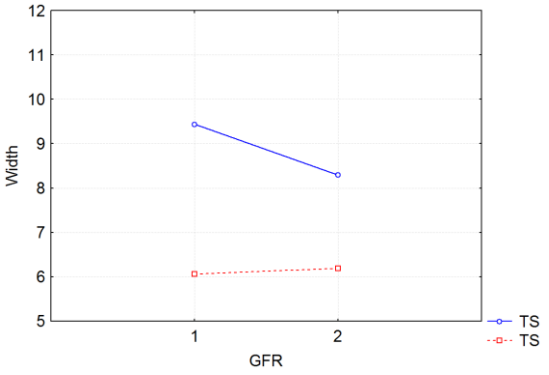

Figure 4.21 Interaction between GFR and TS in continuous wave mode

Concerning the waviness, pulsed wave mode leads to a more dispersed waviness, that is, high values of standard deviation, which indicate that it is a low controllable response, where the only significant parameter is the travel speed (Figure 4.22).

However, in continuous wave mode, most of the specimens present lower standard deviation values of waviness. Both wire feed speed and gas type are significant parameters (Figure 4.23).

As known from welding theory, a mixture of argon-helium-carbon dioxide allows a good spray transfer mode and improves the arc stability. So, with spray transfer mode and a stable arc the waviness is reduced. Similar to other AM processes, in WAAM the waviness is directly related to the thickness of each layer. The reduction of the wire feed speed reduces the height of each layer, thus the waviness decrease.

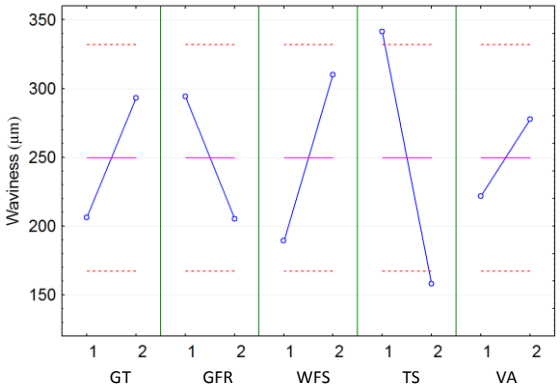

Figure 4.22 Effect of process parameters on waviness in pulsed wave mode

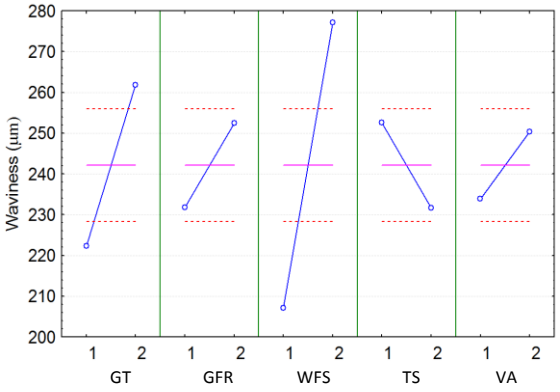

Figure 4.23 Effect of process parameters on waviness in continuous wave mode

It is obvious that the wire feeding speed directly affects the deposition rate. The remaining parameters do not show a significant influence when compared to the WFS. The design of experiments showed that there is no relevant difference between continuous and pulsed wave mode, when the response is the deposition rate (Figure 4.24 and 4.25).

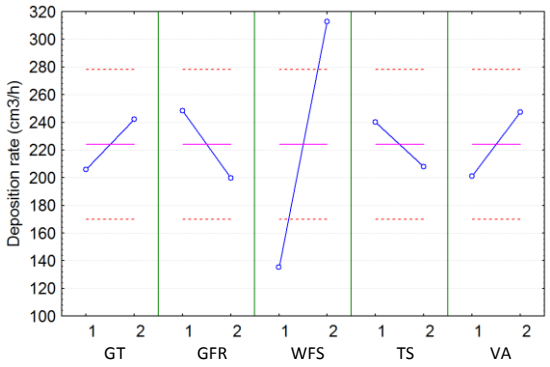

Figure 4.24 Effect of process parameters on deposition rate in pulsed wave mode

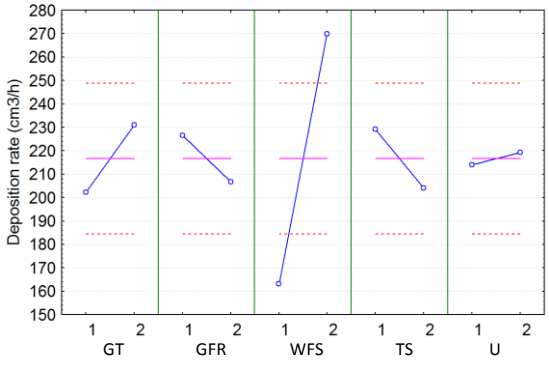

Figure 4.25 Effect of process parameters on deposition rate in continuous wave mode

Since the deposition rate is one of the most important advantages of WAAM and the waviness the major disadvantage, the objective is to minimize the waviness and maximize the deposition rate. However, it is not possible to achieve the optimum value of both waviness and deposition rate with the same set of parameters, that is, most of the parameters have the same effect which can be of

decreasing or increasing both responses. Thereby, knowing that deposition rate is mainly controlled by increasing the wire feeding speed and, that waviness can be minimised by decreasing it, a balance in the WFS set must be achieved.

Finally, and to evaluate the significance of the parameters used in the process, analysis of variance (ANOVA) was applied. The results of the analysis were obtained through the ANOVA table for each studied response. These tables indicate the most relevant processing parameter through the sources that contribute to the total variation in the data values.

The results showed consistency with the physical process and were similar to the ones previously presented. It should be noticed that the significant parameters found were the same for all the responses, namely: width, waviness and deposition rate. Therefore, Table 4.4 corresponds to the ANOVA table obtained for the width response, as an example since it was similar to the remaining responses. Where SS is the sum of squares, MS is the mean square and F-value and p-value are both statistical tests.

Table 4.4 Analysis of variance (ANOVA) for the width parameter

Effect	SS	MS	F	p
GT	0.24938	0.24938	1.2553	0.463889
GFR	2.86845	2.86845	14.4391	0.163822
WFS	39.23348	39.23348	197.4918	0.045225
TS	41.57621	41.57621	209.2845	0.043936
VA	2.64334	2.64334	13.3059	0.170340
Residual	0.19866	0.19866		

4.3 Depositions with low alloy high strength steel wire

The processing parameters were set, as described in section 3.6, according to the orthogonal array of Taguchi methodology. Table 4.5 presents the parameters used to produce the samples in synergic pulsed wave and continuous wave mode, respectively.

Figure 4.26 to 4.35 depicts the transversal section profiles of the deposits.

Table 4.5 Process parameters of samples in synergic pulsed wave mode and continuous wave mode

Synergic pulsed wave mode					
Sample	Gas	Flow rate (l/min)	WFS (m/min)	TS (mm/s)	Voltage adjustment
AP1	Arcal 121	8	2.5	3.8	-6
AP2	Arcal 121	8	2.5	9.0	+6
AP3	Arcal 121	16	5.5	3.9	-6
AP4	Arcal 121	16	5.5	9.0	+6
AP5	Alphagaz 1	8	5.5	3.8	+6
AP6	Alphagaz 1	8	5.5	9.0	-6
AP7	Alphagaz 1	16	2.5	3.8	+6
AP8	Alphagaz 1	16	2.5	9.0	-6
Continuous wave mode					
Sample	Gas	Flow rate (l/min)	WFS (m/min)	TS (mm/s)	Voltage (V)
AC1	Arcal 121	8	3.0	3.9	21.0
AC2	Arcal 121	8	3.0	9.0	26.0
AC3	Arcal 121	16	5.0	3.9	21.0
AC4	Arcal 121	16	5.0	9.0	26.0
AC5	Alphagaz 1	8	5.0	3.8	26.0
AC6	Alphagaz 1	8	5.0	9.0	21.0
AC7	Alphagaz 1	16	3.0	3.8	26.0
AC8	Alphagaz 1	16	3.0	9.0	21.0

Figure 4.26 AP2 transversal section

Figure 4.27 AP3 transversal section

Figure 4.28 AP4 transversal section

Figure 4.29 AP7 transversal section

Figure 4.30 AP8 transversal section

Figure 4.31 AC1 transversal section

Figure 4.32 AC2 transversal section

Figure 4.33 AC3 transversal section

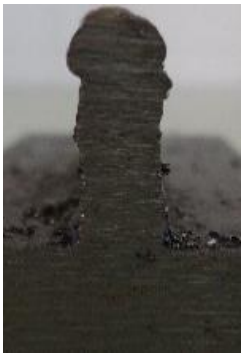

Figure 4.34 AC6 transversal section

Figure 4.35 AC8 transversal section

In each sample, five measurements of width, height and waviness were performed. Average and standard deviations are presented in Table 4.6. The heat input and deposition rate were calculated and the table depicts these values as well as an identification of the samples with porosity.

Table 4.6 Samples results: width, height per layer, waviness, deposition rate, heat input and porosity

	Width (mm) μ±σ	Height per layer (mm) μ±σ	Waviness (μm) μ±σ	Deposition rate (cm^3/h)	Heat Input (J/mm)	Porosity
AP1	7.52±0.26	1.55±0.04	271.1±74.4	1.25	353,6	Yes
AP2	4.99±0.09	0.77±0.03	109.4±60.0	0.96	201,0	No
AP3	10.72±0.13	1.61±0.05	268.7±115.4	1.85	676,5	No
AP4	7.37±0.12	1.28±0.04	175.3±51.22	2.36	297,6	No
AP5	14.23±0.55	2.18±0.11	574.2±190.8	3.33	792,6	Yes
AP6	6.74±0.12	1.31±0.01	221.7±96.83	2.21	242,7	Yes
AP7	6.8±0.29	1.45±0.04	250.8±99.97	1.06	409,5	No
AP8	3.86±0.09	0.99±0.01	125.8±42.45	0.96	134,8	No
AC1	7.14±0.16	1.61±0.01	169.52±64.8	1.24	521,8	No
AC2	6.15±0.46	0.80±0.03	184.46±55.5	1.24	194,5	No
AC3	8.53±0.34	2.26±0.03	279.72±51.4	2.07	554,4	No
AC4	7.42±0.25	0.95±0.03	255.72±86.7	1.76	300,2	Yes
AC5	11.73±1.24	2.00±0.07	306.08±34.3	2.53	667,2	Yes
AC6	5.98±0.13	1.38±0.01	267.04±61.3	2.07	209,5	No
AC7	8.06±0.10	1.52±0.03	254.96±127.	1.32	457,7	No
AC8	4.97±0.10	1.04±0.01	219.36±43.8	1.30	155,0	No

Figure 4.36 and 4.37 depicts the difference between continuous wave mode and pulsed wave mode, with the measurements obtained from sample AC2 and AP2, respectively.

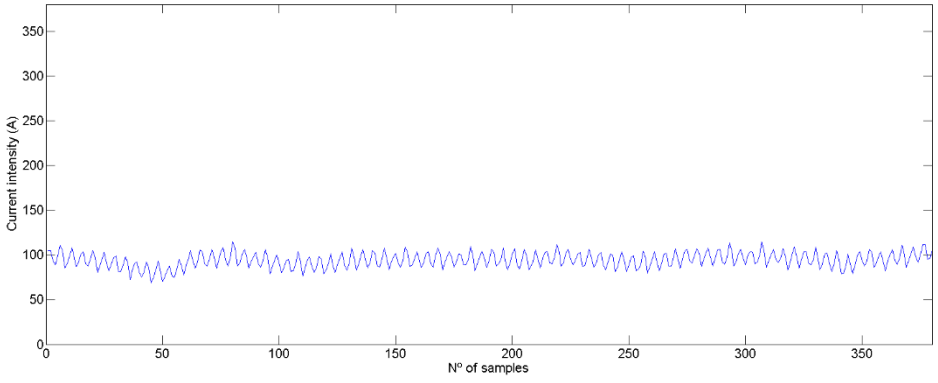

Figure 4.36 Continuous current wave form measured on sample AC2

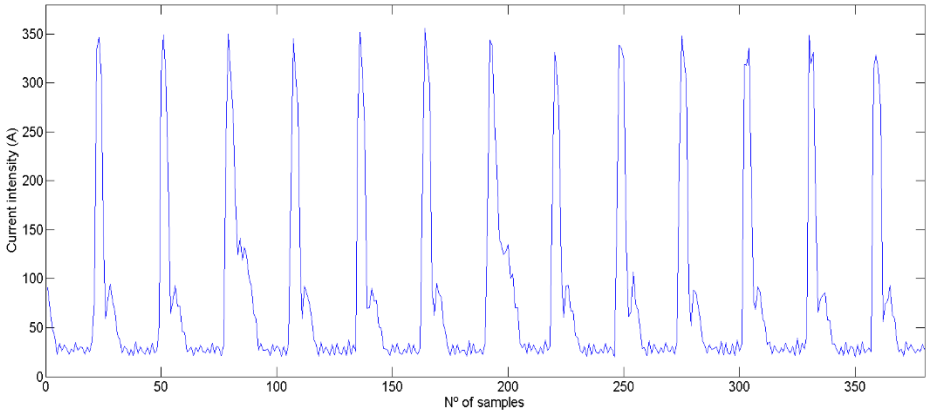

Figure 4.37 Pulsed wave form measured on sample AP2

After a proper adjustment of the processing parameters, defects as humps and valleys were suppressed.

Sample AP5, which corresponded to the one with a higher heat input showed a large weld bead that poured over the substrate, showing a large number of big pores since the gas was dissolved into the molten pool and the deposit was not sufficiently protected by the shielding gas. This result indicate that the heat input had to be reduced as the layers were irregular and the process was not stable.

In a first observation of the results, the continuous wave mode leads to a more stable deposition with a low standard deviation of the waviness. Additionally, waviness increase for higher and larger deposits, as expected, since the stability of previous depositions decrease, not only due to geometrical reasons but also because of the number of thermal cycles introduced, which plasticise the material below Figure 4.38 and 4.39 depict these features.

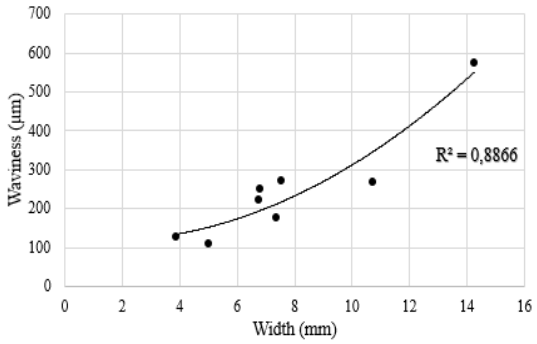

Figure 4.38 Dependence of waviness on width

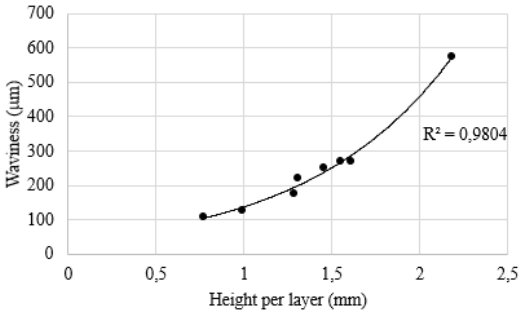

Figure 4.39 Dependence of waviness on height per layer

4.3.1 Microstructure

Similar to preliminary tests, the microscopic observations performed on the specimens revealed the same distinct zones. Associated with the last layer deposited, is an upper region in all the samples which corresponds to the fusion zone (FZ) showing the solidification structure. Below is a gradient of microstructures with different constituents depending on austenitization conditions and cooling

rate. Figure 4.40 show a comparison between samples with low heat input (AP8) and high heat input (AP3).

In both specimens an epitaxial grain growth was observed, perpendicular to the re-melted zone. Comparatively to the preliminary tests, thinner columnar grains were observed and some samples exhibited dendritic structures.

In sample AP3 the microstructure is predominantly constituted by ferrite and pearlite. The darker colour of sample AP8 suggest the presence of more unstable micro constituents, such as bainite or martensite. This is also confirmed by the high hardness values measured on this sample, which were of about 310 HV.

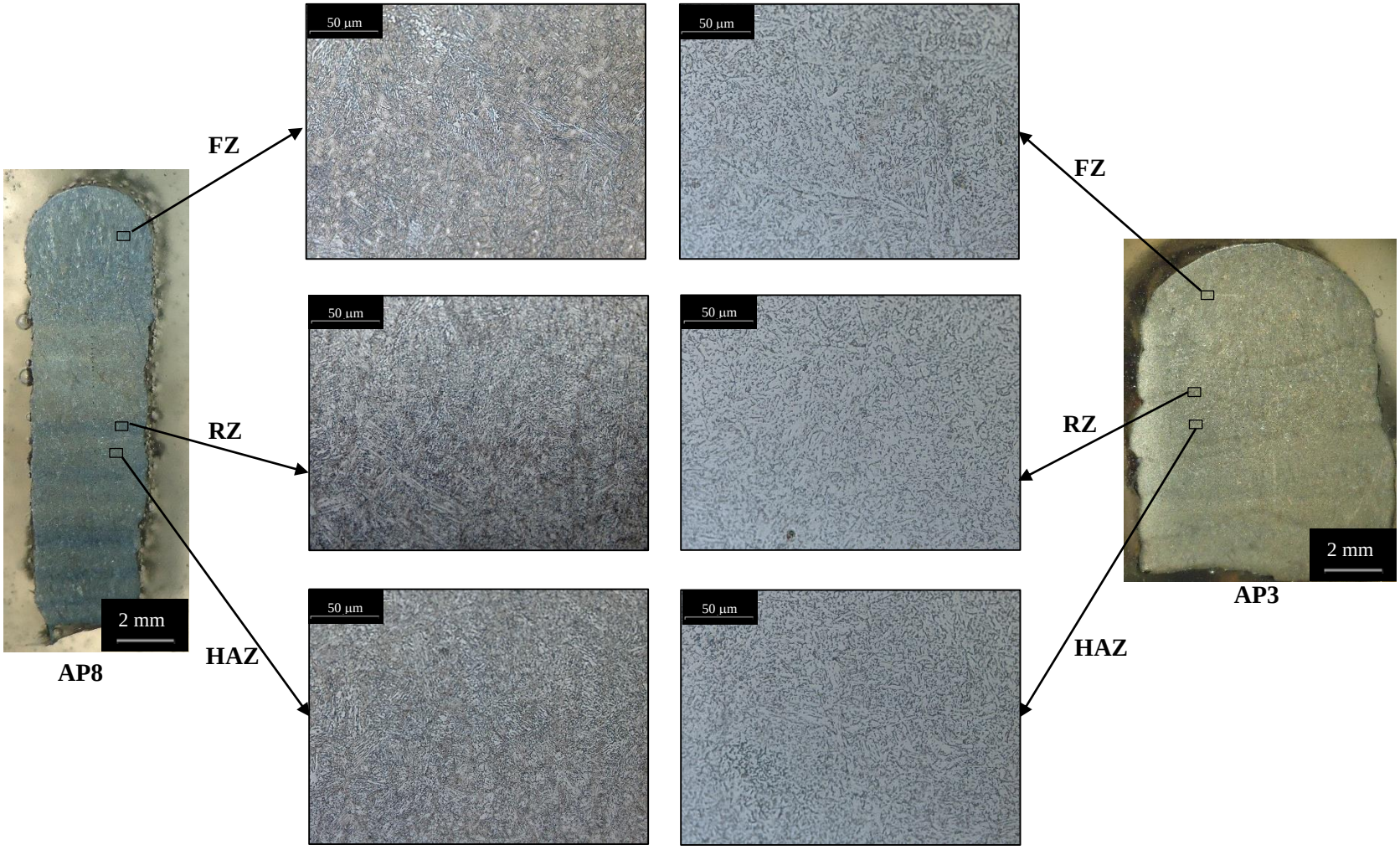

Figure 4.40 Microstructure comparison of samples with different heat input values

4.3.1 Microhardness

Opposite to the preliminary tests, most of the samples present a smooth hardness profile from bottom to top along a vertical line in the center (Figure 4.41). The highest and lowest measured values were 363 HV and 227 HV. The first one are characteristic of martensite while the later are typical of ferrite and perlite microstructures.

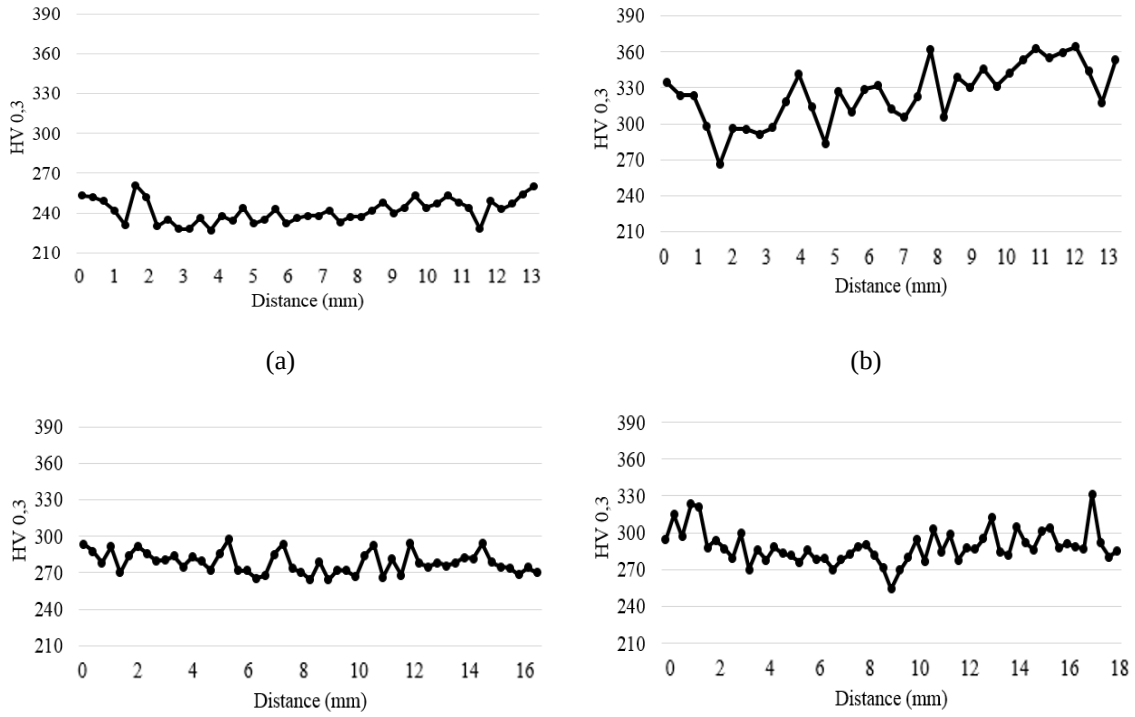

Figure 4.41 Microhardness profile of sample AP3 (a), AP8 (b), AC7 (c) and AC8 (d)

It was seen that samples produced with a low heat input, such as AP8 and AC8, present higher hardness values, and increasing the HI the hardness tends to decrease.

Considering the maximum calculated value of hardness Vickers in section 3.1, most of the samples have slightly lower hardness values. However, in those that have lower heat input the hardness increases to higher values. This relation between the hardness and the heat input is due to the cooling rate. As well known from welding theory, low heat input promotes high cooling rates.

Regarding the material, transformation of austenite varies according to the cooling rate. As an example, martensite is typical of high cooling rates, while ferrite and perlite are typical of low cooling

rates. Nevertheless, the transformation of austenite is also dependent of the material chemical composition.

4.3.2 Uniaxial tensile tests

Uniaxial tensile tests were performed on selected samples without macroscopic defects. Fracture always occurred in the central region of the specimen (Figure 4.42). Ultimate tensile strength and elongation to fracture were calculated and are presented in Table 4.7. For comparison, data from wire test is also given, as well as data of deposited metal provided by the electrode manufacturer.

Figure 4.42 Specimen after uniaxial tensile test

Table 4.7 Strength and ductility parameters from tensile tests results

Sample Reference	UTS [MPa]	Elongation to fracture [%]
AP2	792	15.5
AP3	723	21.6
AP4	762	21.0
AP7	798	19.5
AP8	979	24.1
AC1	1262	12.4
AC2	893	18.4
AC3	773	15.9
AC6	851	16.9
AC7	787	16.9
AC8	914	17.0
Wire	1560	4.4
Weld metal [56]	790	20

The technical specification of the weld metal for this electrode shows an ultimate tensile strength of 790 MPa and an elongation to fracture of 20 %. Analysing the UTS, most of the samples presented values above this, being the lowest observed in AP3 and this was of 723 MPa. However, the elongation to fracture is frequently lower than the one in the technical specification.

In fact, increasing hardness, increases the material strength and ductility decreases.

However, it must be noticed that sample AP8 showed an UTS of 979 MPa of UTS and 24 % of elongation at fracture. That is, the deposited material has a very good strength without loosing ductility, which can be very interesting for industrial applications. Nevertheless, resilience tests or Charpy tests should be performed to assess the toughness of the deposition.

4.3.3 Fractography

After the uniaxial tensile tests, fractography was performed on sample AP8. The SEM observations allow to understand the fracture morphology. Figure 4.43 shows the fracture surface of this sample at various magnifications. A roughened surface with dimples of different sizes was observed. The formation of these dimples occurs due to the plastic deformation of the borders of the solidification grains characteristic of a ductile type fracture.

The grain size is also very small as already seen from the micrographs, confirming the good strength measured.

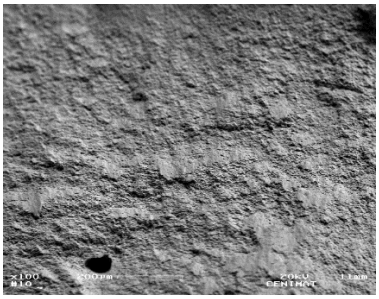

(a)

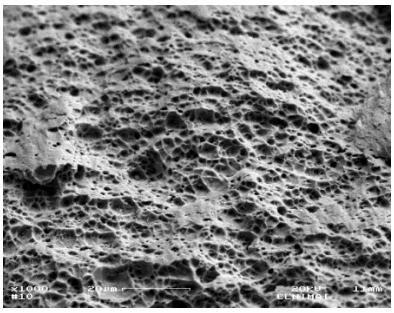

(b)

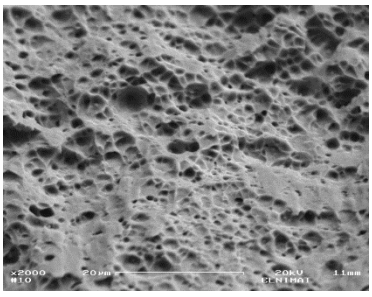

(c)

Figure 4.43 Fracture surfaces from uniaxial tensile test specimen. (a) 200x magnification, (b) 1000x magnification and (c) 2000x magnification

4.3.4 Energy-dispersive X-ray spectroscopy

In order to evaluate the homogeneity of the deposited material, EDS analysis was performed along a vertical line on the AP8 specimen.

Chemical compositions were measured in 7 distinct points shown in Figure 4.44, with a distance of 0.3 mm between each point in order to cover the gradient of microstructures from the fusion zone of one layer till the fusion zone of the adjacent one (Table 4.8).

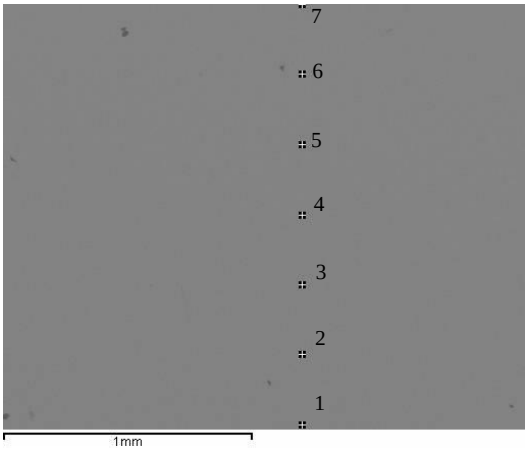

Figure 4.44 EDS analysed points

Table 4.8 EDS analysis results

	wt. %								
	1	2	3	4	5	6	7	Average	Standard deviation
Si	0,52	0,5	0,52	0,53	0,51	0,57	0,55	0,53	0,024
V	0,12	0,1	0,07	0,12	0,06	0,11	0,1	0,10	0,024
Cr	0,37	0,34	0,32	0,29	0,35	0,38	0,34	0,34	0,030
Mn	1,41	1,32	1,34	1,39	1,44	1,49	1,45	1,41	0,06
Ni	1,31	1,17	1,35	1,32	1,22	1,49	1,27	1,30	0,10
Cu	0,19	0,22	0,08	0,09	0,09	0,13	0,07	0,12	0,06
Mo	0,42	0,24	0,23	0,15	0,32	0,27	0,36	0,28	0,09
Fe	93,88	93,42	93,97	93,59	93,67	92,8	93,37	93,53	0,39

It is possible to conclude that the deposited material presents a good homogeneity along the height, with a composition similar to the consumable wire. Carbon was not analysed since under EDS the low energy of carbon x-ray K line, make it easy to be absorbed. Its low energy also means that analysis deepness is reduced and only the carbon x-rays from the surface of the specimen can be counted. Furthermore, there can be a significant carbon background signal, since hydrocarbons from

the chamber surfaces, vacuum pump and sample surface can migrate and react with the electron beam to form a black spot that is rich in carbon [57].

During the fractography analysis, several inclusions with a spherical shape were detected inside the dimples, as shown in Figure 4.45. Focusing the beam on these inclusions, it was seen they were MnS which agrees with existing information about their morphology. MnS is roundish, opposite to FeS, and so is less prone to cracking (Figure 4.46 and 4.47): EDS values are shown in Table 4.9.

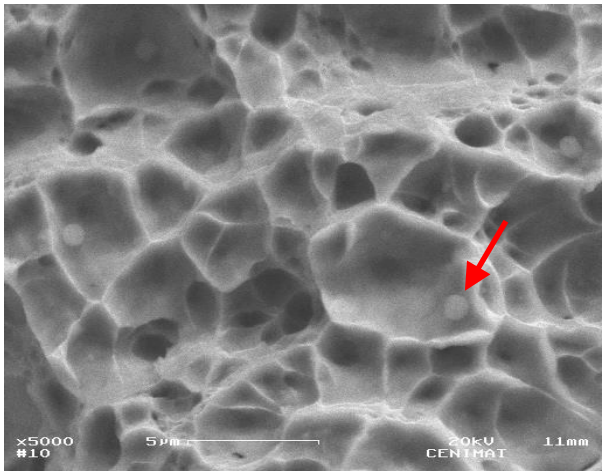

Figure 4.45 Manganese Sulphides inclusions

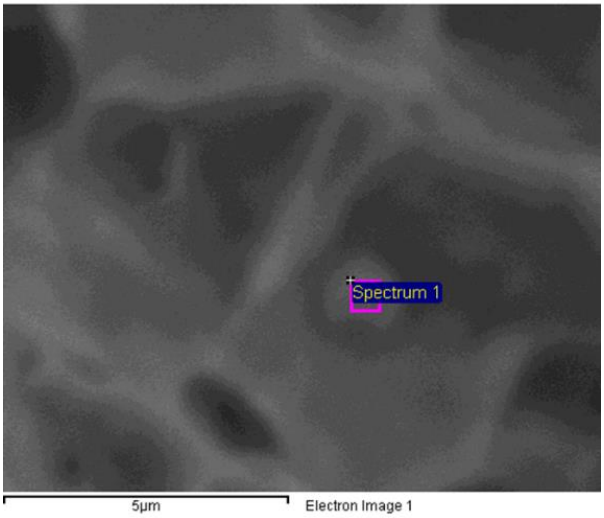

Figure 4.46 Positioning of EDS analysis on sulphide manganese inclusion

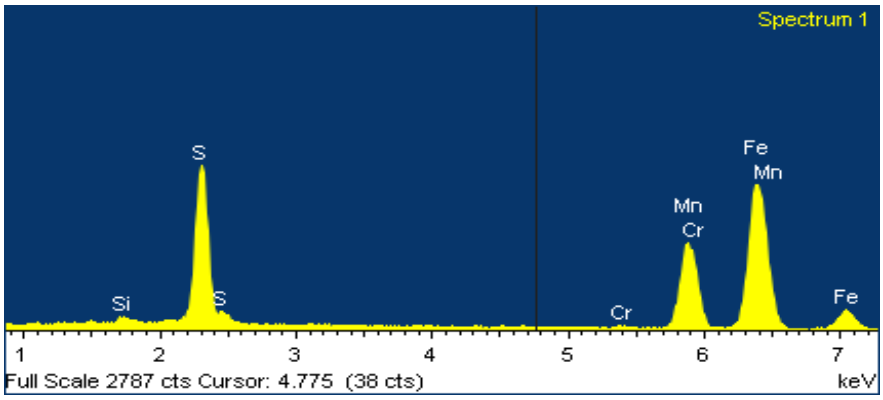

Figure 4.47 EDS spectrum of Manganese sulphur

Table 4.9 EDS result from the analyse of inclusions

	Weight%	**Atomic%**
Si	0.76	1.32
S	17.61	26.84
Cr	0.43	0.41
Mn	27.11	24.13
Fe	53.07	46.46
Ni	1.02	0.85

Besides iron, sulphur and manganese are the predominant elements of the inclusion. This indicates that the inclusions are sulphides of manganese. Moreover, knowing that MnS is a heteronuclear diatomic molecule the sulphur atomic % is expected to be similar of the Mn atomic %, which is confirmed by the results. Despite the technical specifications of the consumable rod do not indicate the presence of sulphur, it is known that elements such as sulphur and phosphor are very difficult to remove from a carbon steel alloy, thus the sulphur source is almost certainly the consumable electrode.

Presence of sulfides of manganese is common in steels unless treated with rare earth metals [58]. In electrode welding consumables the Mn content is frequently more than 0.30%. because it assists in the deoxidation of the steel, prevents the formation of iron sulphide by grabbing the sulphur element and form manganese sulphide. Manganese also have affinity with oxygen and form stable oxides, which helps control the loss of alloying elements through oxidation and the formation of carbon monoxide, which otherwise could cause porosity. The presence of manganese also promotes greater strength by increasing the hardness of the steel [46].

4.3.5 X-ray diffraction

X-ray difraction analysis revealed the prensece of manganese sulphides and iron, identified on Figure 4.48. The remain peaks on the spectrum are iron-based oxides.

Trougthout the several analysed point in each sample, homegenety characteristics were observed. Moreover, all the analysed samples presented similar characteristics (Figure 4.49 to 4.51).

Additionally, the results also allow to confirm the presence of MnS indentified on the SEM observations analysis.

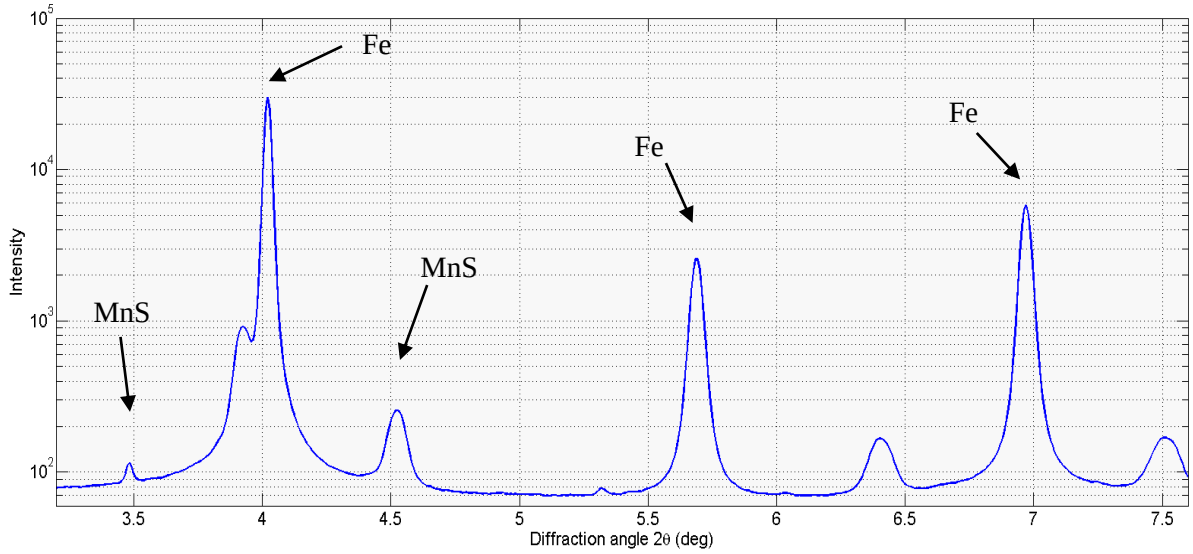

Figure 4.48 One zone spectrum of XRD analysis in sample AC1

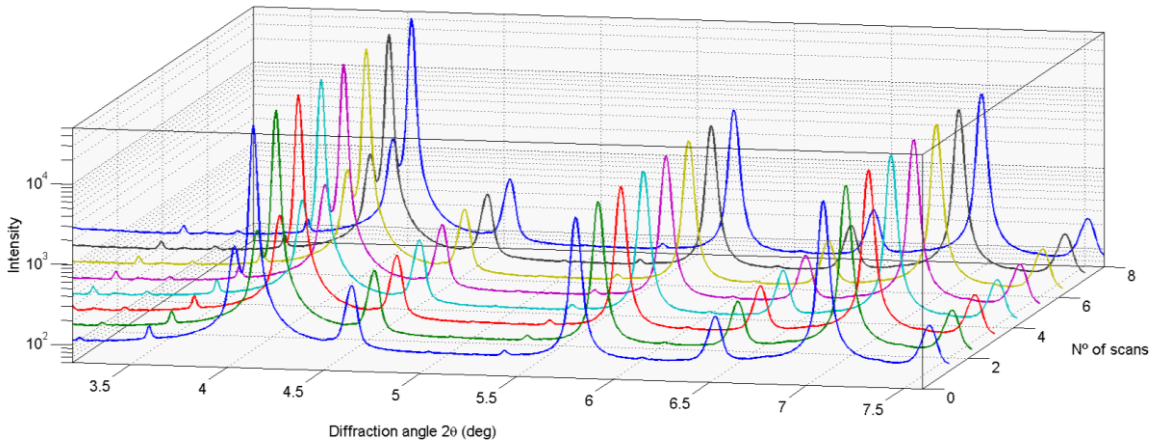

Figure 4.49 Multiple XRD analysis in sample AP2

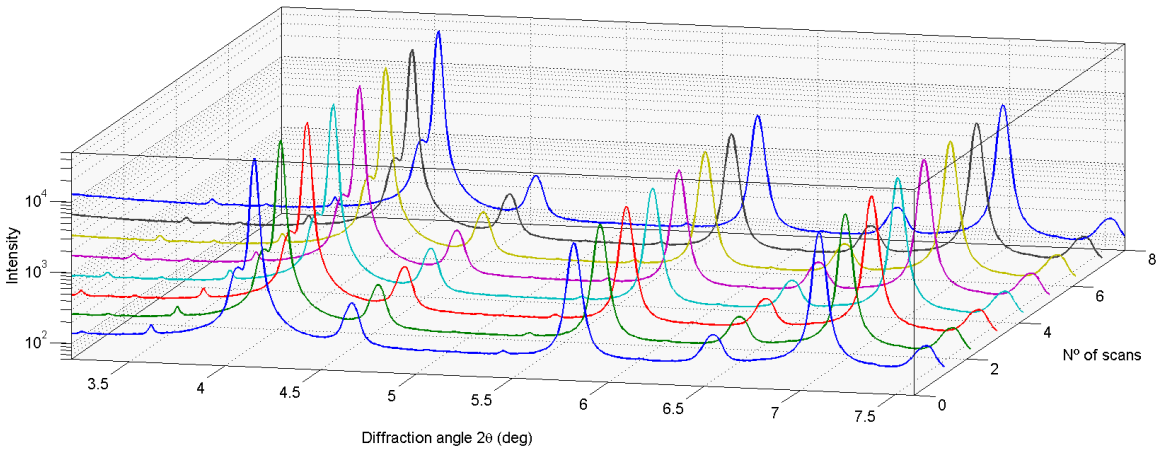

Figure 4.50 Multiple XRD analysis in sample AP8

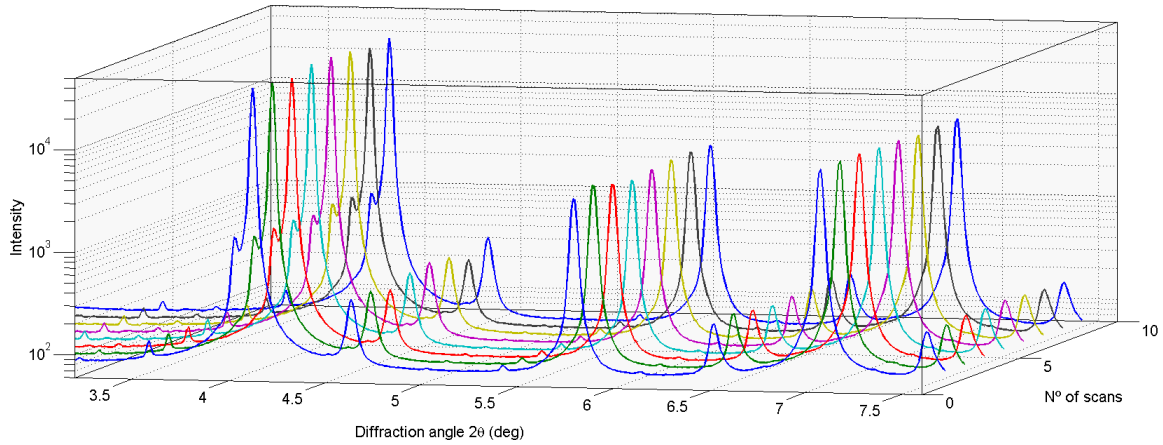

Figure 4.51 Multiple XRD analysis in sample AC8

5

Conclusions and future work

Wire and Arc Additive Manufacturing of low alloy steel, ER110G-S, has been developed during this study. The proposed objectives were achieved and the following can be concluded:

1. Metal inert gas process is appropriate for wire and arc additive manufacturing applications based upon deposition characteristics and process behaviour.
2. Weld bead humping defect occurs at high travel speeds, but can be smoother increasing of the wire feed speed.
3. In continuous wave mode the waviness is more regular with less spatter. However, the lowest values were obtained in depositions made in pulsed wave mode and were of 109.4 μm, which represent a very significant result when compared with other WAAM studies where the waviness values are between 150 μm and 3 mm. [26-29,40]
4. Waviness is directly affected by the width and height of each layer.
5. Uniaxial tensile tests showed tensile strength values between 723 and 1262 MPa, which are in most of the cases above the resistance provided by the wire manufacturer. Sample AP8 showed an UTS of 979 MPa and 24 % of elongation at fracture which represent a very good strength of the deposited material without loosing ductility. Additionally, these values have shown to be consistent with the indentation hardness profiles.
6. The microstructure refinement is directly affected by the heat input and it was fully compacted without pores in most of the samples and no cracks.
7. EDS results revealed a homogenous chemical composition of the deposited material, along the height, which means that there is no loss of alloying elements which is in agreement with the mechanical resistance registered.
8. The process deposition rate ranged from 123 to 427 cm^3/h which is highly above the ones achieved with powder feeding systems and is slightly above of the common values of wire feed processes [5].

After the promising results and aiming at developing additive manufacturing using wire and arc additive manufacturing up to TRLs close to industrialization a long process is still to be performed.

Nevertheless, research is needed specially in the following areas:

1. Deeper mechanical characterization, specifically on the uniaxial tensile test with samples obtained from different orientation, in order to evaluate the isotropic characteristics of the deposited material and Charpy tests to assess the toughness of the part;
2. Produce parts with more complex geometries and characterization to assess the effect of deposition rates and sequences;
3. Use other materials for producing parts;
4. Study of the formation of the fine dendrites inside the irregularities identified

References

[1] ASTM F2792-12a:2012, *Standard Terminology for Additive Manufacturing Technologies*. ASTM International, West Conshohocken, PA, 2012.

[2] Nannan GUO, Ming C. LEU, *Additive manufacturing: technology, applications and research needs*, Frontiers of Mechanical Engineering 8 (2013), pp. 215–243.

[3] Kaufui V. Wong, Aldo Hernandez, *A Review of Additive Manufacturing*, *ISRN Mechanical Engineering*, 2012.

[4] C. Weller, R. Kleer, and F. T. Piller, *Economic implications of 3D printing: Market structure models in light of additive manufacturing revisited*, International Journal of Production Economics 164 (2015), pp. 43–56.

[5] D. Ding, Z. Pan, D. Cuiuri, and H. Li, *Wire-feed additive manufacturing of metal components: technologies, developments and future interests*, Int J Adv Manuf Technol 81 (2015), pp. 465–481.

[6] E. Uhlmann, R. Kersting, T. B. Klein, M. F. Cruz, and A. V. Borille, *Additive Manufacturing of Titanium Alloy for Aircraft Components*, *Procedia CIRP* 35 (2015) pp. 55–60.

[7] G. J. Schiller, *Additive manufacturing for Aerospace*, 2015 IEEE Aerospace Conference (2015) pp. 1–8.

[8] J. Giannatsis and V. Dedoussis, *Additive fabrication technologies applied to medicine and health care: a review*, Int J Adv Manuf Technol 40 (2007) pp. 116–127.

[9] S. C. Cox, P. Jamshidi, N. M. Eisenstein, M. A. Webber, H. Hassanin, M. M. Attallah, D. E. T. Shepherd, O. Addison, and L. M. Grover, *Adding functionality with additive manufacturing: Fabrication of titanium-based antibiotic eluting implants*, Materials Science and Engineering*:*64 (2016) pp. 407–415.

[10] J-P. Kruth, P. Mercelis, J. Van Vaerenbergh, L. Froyen, and M. Rombouts, *Binding mechanisms in selective laser sintering and selective laser melting*, Rapid Prototyping Journal, 11 (2005) pp. 26–36.

[11] G. N. Levy, R. Schindel, and J. P. Kruth, *Rapid manufacturing and rapid tooling with layer manufacturing (LM) technologies, state of the art and future perspectives*, CIRP Annals - Manufacturing Technology 52 (2003) pp. 589–609.

[12] William E. Frazier, *Metal Additive Manufacturing: A Review*, Journal of Materials Engineering and Performance 23 (2014) pp. 1917–1928.

[13] R. M. Miranda, G. Lopes, L. Quintino, J. P. Rodrigues, and S. Williams, *Rapid prototyping with high power fiber lasers*, Materials & Design 29 (2008) pp. 2072–2075.

[14] E. Brandl, A. Schoberth, and C. Leyens, M*orphology, microstructure, and hardness of titanium (Ti-6Al-4V) blocks deposited by wire-feed additive layer manufacturing (ALM)* 532 (2012) pp. 295–307.

[15] B. Baufeld, O. V. der Biest, and R. Gault, *Additive manufacturing of Ti–6Al–4V components by shaped metal deposition: Microstructure and mechanical properties*, Materials & Design 31 (2010) pp. S106–S111.

[16] F. Klock, H. Wirtz, *Selective Laser Sintering of Zirconium Silicate*, Fraunhofer Institute of Production Technology IPT, 1998.

[17] J. Mazumder, J. Choi, K. Nagarathnam, J. Koch, and D. Hetzner, *The direct metal deposition of H13 tool steel for 3-D components*, The Journal of the Minerals 49 (1997) pp. 55–60.

[18] G. Nicoletto, S. D. Pastrama, I. Emri, A. Bača, R. Konečná, G. Nicoletto, and L. Kunz, *32nd Danubia Adria Symposium on Advances in Experimental Mechanics Influence of Build Direction on the Fatigue Behaviour of Ti6Al4V Alloy Produced by Direct Metal Laser Sintering*, Materials Today: Proceedings 3 (2016) pp. 921–924.

[19] Mukesh Agarwala, David Bourell, Joseph Beaman, Harris Marcus, and Joel Barlow, *Direct selective laser sintering of metals*, Rapid Prototyping Journal 1 (1995) pp. 26–36.

[20] J.P. Kruth, X. Wang, T. Laoui, and L. Froyen, *Lasers and materials in selective laser sintering*, Assembly Automation 23 (2003) pp. 357–371.

[21] M. Schmidt, M. Zaeh, T. Graf, A. Ostendorf, D. Buchbinder, H. Schleifenbaum, S. Heidrich, W. Meiners, and J. Bültmann, *Lasers in Manufacturing 2011 - Proceedings of the Sixth International WLT Conference on Lasers in ManufacturingHigh Power Selective Laser Melting (HP SLM) of Aluminum Parts*, Physics Procedia 12 (2011) pp. 271–278.

[22] G. Strano, L. Hao, R. M. Everson, and K. E. Evans, *Surface roughness analysis, modelling and prediction in selective laser melting*, Journal of Materials Processing Technology 213 (2013) pp. 589–597.

[23] S. Bremen, W. Meiners, and A. Diatlov, *Selective Laser Melting*, *Laser Technik Journal* 9 (2012) pp. 33–38.

[24] F. Abe, K. Osakada, M. Shiomi, K. Uematsu, and M. Matsumoto, *The manufacturing of hard tools from metallic powders by selective laser melting*, Journal of Materials Processing Technology 111 (2001) pp. 210–213.

[25] Zhai Yuwei, Galarraga Haize, Lados Diana A., *Microstructure, static properties, and fatigue crack growth mechanisms in Ti-6Al-4V fabricated by additive manufacturing: LENS and EBM*, Engineering failure analysis 2016.

[26] T. Abe and H. Sasahara, *Dissimilar metal deposition with a stainless steel and nickel-based alloy using wire and arc-based additive manufacturing*, Precision Engineering 45 (2016) pp. 387–395.

[27] Panagiotis Kazanas, Preetam Deherkar, Pedro Almeida, Helen Lockett, and Stewart Williams, *Fabrication of geometrical features using wire and arc additive manufacture*, Journal of Engineering Manufacture 226 (2012) pp. 1042–1051.

[28] Y.-A. Song, S. Park, D. Choi, and H. Jee, *3D welding and milling: Part I–a direct approach for freeform fabrication of metallic prototypes*, International Journal of Machine Tools and Manufacture 45 (2005) pp. 1057–1062.

[29] Y.-A. Song, S. Park, and S.-W. Chae, *3D welding and milling: part II—optimization of the 3D welding process using an experimental design approach*, International Journal of Machine Tools and Manufacture 45 (2005) pp. 1063–1069.

[30] F. Wang, S. Williams, and M. Rush, *Morphology investigation on direct current pulsed gas tungsten arc welded additive layer manufactured Ti6Al4V alloy*, Int J Adv Manuf Technol 57 (2011) pp. 597–603.

[31] D. Ding, Z. Pan, D. Cuiuri, and H. Li, *A practical path planning methodology for wire and arc additive manufacturing of thin-walled structures*, Robotics and Computer-Integrated Manufacturing 34 (2015) pp. 8–19.

[32] D. Ding, C. Shen, Z. Pan, D. Cuiuri, H. Li, N. Larkin, and S. van Duin, *Towards an automated robotic arc-welding-based additive manufacturing system from CAD to finished part*, Computer-Aided Design 73 (2016) pp. 66–75.

[33] J. Xiong, G. Zhang, H. Gao, and L. Wu, *Modeling of bead section profile and overlapping beads with experimental validation for robotic GMAW-based rapid manufacturing*, Robotics and Computer-Integrated Manufacturing 29 (2013) pp. 417–423.

[34] S. Suryakumar, K. P. Karunakaran, A. Bernard, U. Chandrasekhar, N. Raghavender, and D. Sharma, *Weld bead modeling and process optimization in Hybrid Layered Manufacturing*, Computer-Aided Design 43 (2011) pp. 331–344.

[35] Y. Cao, S. Zhu, X. Liang, and W. Wang, *Overlapping model of beads and curve fitting of bead section for rapid manufacturing by robotic MAG welding process*, Robotics and Computer-Integrated Manufacturing 27 (2011) pp. 641–645.

[36] J. Xiong, G. Zhang, Z. Qiu, and Y. Li, *Vision-sensing and bead width control of a single-bead multi-layer part: material and energy savings in GMAW-based rapid manufacturing*, Journal of Cleaner Production 41 (2013) pp. 82–88.

[37] D. Ding, Z. Pan, D. Cuiuri, H. Li, S. van Duin, and N. Larkin, *Bead modelling and implementation of adaptive MAT path in wire and arc additive manufacturing*, Robotics and Computer-Integrated Manufacturing 39 (2016) pp. 32–42.

[38] Y. Zhang, Y. Chen, P. Li, and A. T. Male, *Weld deposition-based rapid prototyping: a preliminary study*, Journal of Materials Processing Technology 135 (2003) pp. 347–357.

[39] S. Akula and K. P. Karunakaran, *Hybrid adaptive layer manufacturing: An Intelligent art of direct metal rapid tooling process*, Robotics and Computer-Integrated Manufacturing 22 (2006) pp. 113–123.

[40] C. Shen, Z. Pan, Y. Ma, D. Cuiuri, and H. Li, *Fabrication of iron-rich Fe–Al intermetallics using the wire-arc additive manufacturing process*, Additive Manufacturing 7 (2015) pp. 20–26.

[41] A. S. Haselhuhn, B. Wijnen, G. C. Anzalone, P. G. Sanders, and J. M. Pearce, *In situ formation of substrate release mechanisms for gas metal arc weld metal 3-D printing*, Journal of Materials Processing Technology 226 (2015) pp. 50–59.

[42] ASM International, "Welding, Brazing, and Soldering" in: ASM Handbook, Volume 6, ISBN: 0-87170-706-3.

[43] P. Kah, H. Latifi, R. Suoranta, J. Martikainen, and M. Pirinen, *Usability of arc types in industrial welding*, International Journal of Mechanical and Materials Engineering 9 (2014) pp. 1–12.

[44] E. F. da Silva, J. R. M, A. Scotti, and J. C. de Oliveira, *Power quality analysis of gas metal ARC welding process operating under different drop transfer modes*, XI Brazilian Power Electronics Conference (2011) pp. 129–135.

[45] J.F. Oliverira Santos and L. Quintino, "Processos de Soldadura", 2ª ed. ISQ, Lisboa, 1998, ISBN: 972-9228-73-6.

[46] American Welding Society, "Welding Process Part 1" in: Welding Handbook, Volume. 2, Editor: Annette O'Brien, ISBN: 0-87171-729-8.

[47] Americo Scotti, *A Review on Special Metal Transfer Modes in Gas Metal Arc Welding*, J. of the Braz. Soc. Mechanical Sciences 20 (1998) pp. 465–478.

[48] P. K. Palani and N. Murugan, *Selection of parameters of pulsed current gas metal arc welding*, Journal of Materials Processing Technology 172 (2006) pp. 1–10.

[49] C. S. Wu, M. A. Chen, and Y. F. Lu, *Effect of current waveforms on metal transfer in pulsed gas metal arc welding*, Measurement Science and Technology 16 (2005) pp. 2459.

[50] D. Iordachescu, L. Quintino, R. Miranda, and G. Pimenta, *Influence of shielding gases and process parameters on metal transfer and bead shape in MIG brazed joints of the thin zinc coated steel plates*, Materials & Design 27 (2006) pp. 381–390.

[51] J. Kestin, Y. Nagasaka, and W. A. Wakeham, *The thermal conductivity of mixtures of carbon dioxide with three noble gases*, North-Holland Publishing Co.(1982) pp. 1–26.

[52] E. M. D. Lopes and R. M. Miranda, "Metalurgia da soldadura".ed. ISQ, Lisboa, 1993, ISBN: 9729228167.

[53] The Lincoln Electric Company, " LNM MoNiVa ER110S-G consumable electrode technical data" .

[54] D. C. Montgomery, "Design and Analysis of Experiments", 5th ed. John Wiley & Sons, INC., 2001, ISBN: 0-471-31649-0

[55] J. G. Requeijo and Z. L. Pereira, "Qualidade: Planeamento e Controlo Estatístico de Processos". FCT-Prefácio, 2008, ISBN: 978-989-8022-65-3

[56] A. Adebayo, J. Mehnen, and X. Tonnellier, *Limiting travel speed in additive layer manufacturing*, 9th International Conference on Trends in Welding Research (2013).

[57] P. Rolland, V. Carlino, and R. Vane, *Improved Carbon Analysis with Evactron Plasma Cleaning*, Microscopy and Microanalysis (2004) pp. 964–965.

[58] J. M. Dowling, J. M. Corbett, and H. W. Kerr, *Inclusion phases and the nucleation of acicular ferrite in submerged arc welds in high strength low alloy steels*, Metallurgical and Materials Transactions A 17 (1986) pp. 1611–1623.

Appendix A - Uniaxial tensile tests

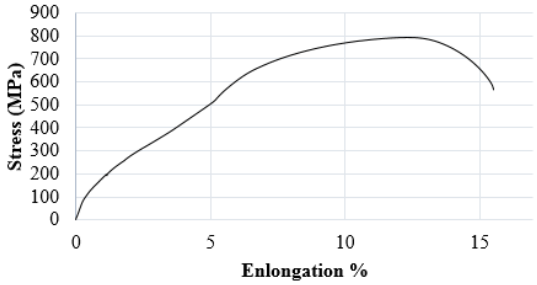

AP2

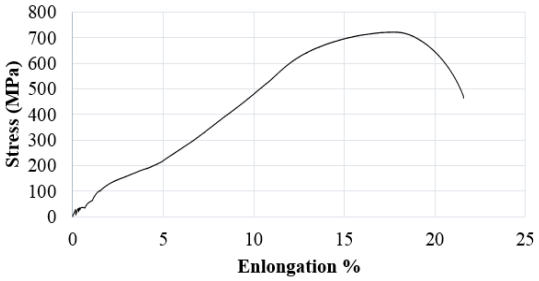

AP3

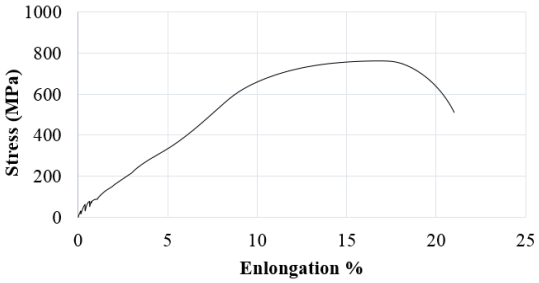

AP4

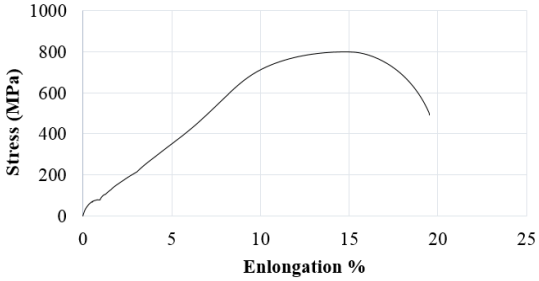

AP7

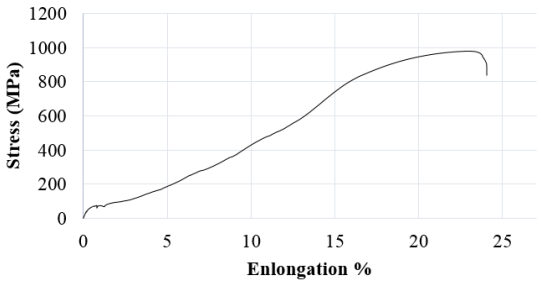

AP8

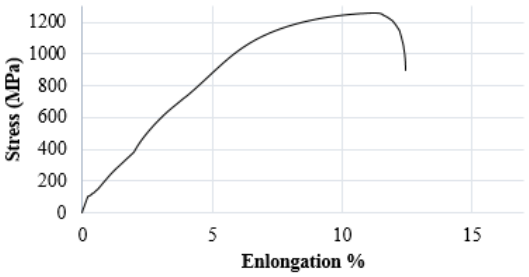

AC1

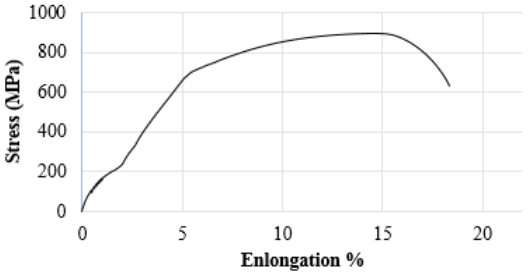

AC2

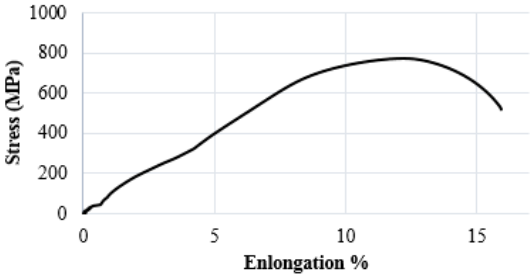

AC3

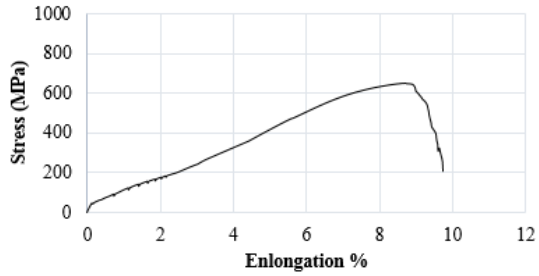

AC4

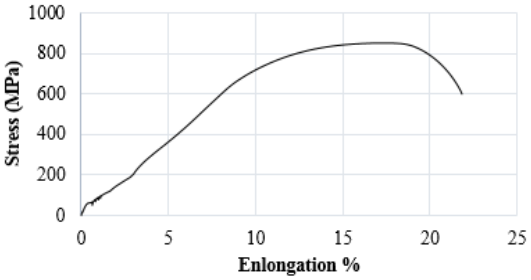

AC6

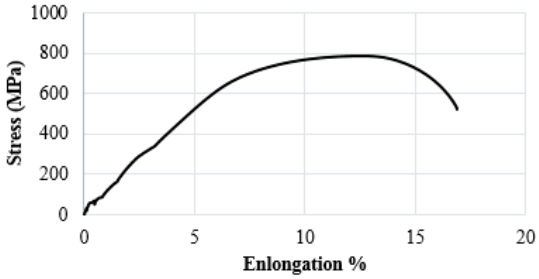

AC7

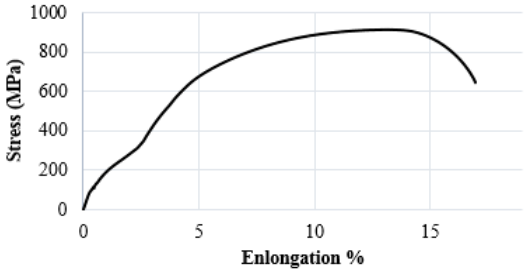

AC8